

AROUND 200 NEW X-RAY BINARY IDS FROM 13 YEARS OF CHANDRA OBSERVATIONS OF THE M31 CENTER

R. BARNARD, M. GARCIA, AND F. PRIMINI
Harvard-Smithsonian Center for Astrophysics, Cambridge, MA 02138

AND

Z. LI
School of Astronomy and Space Science, Nanjing University, Nanjing 210093, China

AND

F. K. BAGANOFF
Center for Space Research, M.I.T., Cambridge, MA 02139

AND

S. S. MURRAY
Johns Hopkins University, Baltimore, Maryland
Draft version October 2, 2018

ABSTRACT

We have created 0.3–10 keV, 13 year, unabsorbed luminosity lightcurves for 528 X-ray sources in the central 20′ of M31. We have 174 Chandra observations spaced at ∼1 month intervals thanks to our transient monitoring program, deeper observations of the M31 nucleus, and some public data from other surveys. We created 0.5–4.5 keV structure functions (SFs) for each source, for comparison with the ensemble structure function of AGN. We find 220 X-ray sources with luminosities $\gtrsim 10^{35}$ erg s^{−1} that have SFs with significantly more variability than the ensemble AGN SF, and are likely X-ray binaries (XBs). A further 30 X-ray sources were identified as XBs using other methods. We therefore have 250 probable XBs in total, including ∼200 new identifications. This result represents great progress over the ∼50 XBs and ∼40 XB candidates previously identified out of the ∼2000 X-ray sources within the D₂₅ region of M31; it also demonstrates the power of SF analysis for identifying XBs in external galaxies. We also identify a new transient black hole candidate, associated with the M31 globular cluster B128.

Subject headings: x-rays: general — x-rays: binaries — globular clusters: general — globular clusters: individual

1. INTRODUCTION

The X-ray populations of external galaxies have the potential to provide excellent diagnostics on the evolutionary states of their host galaxies. However, separating the true galaxy population from active galaxies in the field is notoriously difficult. This is because X-ray binaries (XBs) are expected to dominate the X-ray populations of galaxies, and their emission spectra can be very similar to the spectra of active galactic nuclei (AGN). In fact, it has been rather difficult to classify X-ray sources in external galaxies at all; Stiele et al. (2011) examined 1897 X-ray sources within the D₂₅ region for M31, but only identified 46 XBs and 43 XB candidates, while ∼65% of the X-ray sources had no classification. However, we have recently invented a method for discriminating between XBs and AGN by formalizing their differences in variability (Barnard et al. 2012b).

It has long been known that AGN may vary by a factor of 2–3 on time-scales of months to years, with the amplitude of variation inversely proportional to the luminosity (see e.g. Marshall et al. 1981; Nandra et al. 1997, and references within). However, exceptional AGN can flare up by an order of magnitude (e.g. Tananbaum et al. 1978).

Recently Vagnetti et al. (2011) studied the ensemble variability over time-scales of hours to years of AGN

in the serendipitous source catalogs from XMM-Newton (Watson et al. 2009) and Swift (Puccetti et al. 2011); their sample covered red-shifts ∼0.2–4.5, and 0.5–4.5 keV luminosities ∼10⁴³–10⁴⁶ erg s^{−1}. They included 412 AGN from the XMM-Newton catalog, and 27 AGN from the Swift catalog; all of these AGN were sampled at least twice. They used a structure function (SF) to estimate the mean intensity deviation for data separated by time τ :

$$SF(\tau) \equiv \sqrt{\frac{\pi}{2} \langle |\log f_X(t + \tau) - \log f_X(t)|^2 - \sigma_n^2 \rangle}, \quad (1)$$

where σ_n is the photon noise and f_X is the X-ray flux. They grouped the SF into logarithmic bins with width 0.5; each bin in the range $\log(\tau) = 0.0$ –3.0 contained more than 100 measurements.

Vagnetti et al. (2011) found good agreement between the XMM-Newton and Swift samples of AGN, after the noise components were subtracted; $SF(\tau) \propto \tau^{0.10 \pm 0.01}$ for the XMM-Newton sample, and $SF(\tau) \propto \tau^{0.07 \pm 0.04}$ for the Swift sample. They also investigated the well-observed anti-correlation between intensity variability (I_{var}) and luminosity, expressed in the form $I_{\text{var}} \propto L_X^{-k}$; $k \sim 0.3$ in the literature for time-scales of days to tens of days. They measured k for AGN grouped logarithmically over $\log L_X = 43.5$ –45.5 for two values of τ : 1 day and 100

days. They find $k = 0.42 \pm 0.03$ for $\tau = 1$ day, and $k = 0.21 \pm 0.07$ for $\tau = 100$ days; the latter result is consistent with the work of Markowitz & Edelson (2004), who found $k \sim 0.13$ for variations over year-long time-scales.

Recently, Stiele et al. (2008) examined the variability of X-ray sources in the M31 center over 9 deep XMM-Newton observations spanning 2000 June – 2004 July; they obtained fluxes or upper limit for each X-ray source in every observation, and searched for differences between maximum and minimum flux $> 3\sigma$. They found 149 sources out of 300 to exhibit $> 3\sigma$ flux variability; of those, 44 exhibited variability by a factor > 5 , including 28 XBs or XB candidates. Stiele et al. (2008) reclassified any “hard” X-ray source which varied by a factor > 10 as a candidate XB; however, according to the SF obtained by Vagnetti et al. (2011), typical AGN only vary by $\lesssim 70\%$ over 4 years, meaning that further XBs could have been identified in hind-sight from that variability study.

We have been studying the long-term variability of 528 X-ray sources over 174 Chandra observations of the inner regions of M31, taken over ~ 13 years. We conducted a pilot structure function survey, on 37 X-ray sources associated with globular clusters that are probable low mass XBs (Barnard et al. 2012b). We found that the lower luminosity XBs tended to exhibit considerably more variability than the ensemble AGN SF; the higher luminosity XBs exhibited SFs that indicated comparable or lesser variability than the ensemble AGN SF. Such dependence on variation with luminosity is well known in Galactic systems, where the Z-sources (high luminosity XBs) vary only by a factor of a few, while the atoll sources (low luminosity XBs) vary by ~ 1 –2 orders of magnitude (Muno et al. 2002).

In this work we will present an overview of the long-term variability of the 528 X-ray sources in our chosen region, out to $20'$ (~ 4.5 kpc) from the center of M31. We have created 0.5–4.5 keV SFs for each target, for comparison with the ensemble AGN SF created by Vagnetti et al. (2011). With these results, we will place limits on the numbers of XBs and AGN in this region. We will also compare the number of possible AGN with the expected number from the 0.5–10 keV AGN flux distribution created by Georgakakis et al. (2008).

We have previously published detailed studies of 13 X-ray transients with Chandra and HST coverage (Barnard et al. 2012a, 2013b), and of those X-ray sources associated with M31 globular clusters (Barnard et al. 2012b). We also recently published our 26 new black hole candidates that we identified via structure function analysis (Barnard et al. 2013a). Further work on the ~ 50 transients in our study will be presented separately (R. Barnard et al., in prep). In the following sections, we provide details of the observations and data reduction, followed by results and our discussion.

2. OBSERVATIONS AND DATA REDUCTION

The central region of M31 has been observed with Chandra on a \sim monthly basis for the last ~ 13 years in order to monitor transients; we exclude periods when M31 cannot be viewed due to orbital constraints (approximately March–May each year). We have analyzed 112 ACIS observations and 62 HRC observations, in order to discern the variability of X-ray sources in this region.

Initial source detection was performed on a merged ACIS events file created from observations performed in 1999 October–2010 March; the detection procedure followed that outlined by Wang (2004). Each observation was registered to a single coordinate system, with the systematic uncertainty in registration included in the uncertainty in the centroid position in the merged image. The total exposure was 305 ks but the combined effective 0.5–8 keV exposure varied considerably over the field of view, from $\sim 2 \times 10^5$ s in the center to $\sim 1.1 \times 10^5$ s within $6'$ of the center, and down to $\sim 10^4$ ks at larger off-axis angles. The highest sensitivity was found $\sim 2'$ from the nucleus ($\sim 7 \times 10^{-5}$ count s^{-1} , or $\sim 5 \times 10^{34}$ erg s^{-1}); diffuse emission is highly significant within $2'$, while a combination of degrading PSFs and lower exposures decreased the sensitivity by a factor $\gtrsim 20$ at high off-axis angles.

Sources were considered significant if they satisfied one or both of the following criteria. A source was considered significant if the best fit line of constant intensity was $\geq 3\sigma$ above zero; some transient X-ray sources would be rejected by this criterion, so we also accepted sources that demonstrated significant variability.

We compared our initial Chandra source list with the inventory from an XMM-Newton survey of M31 performed by Stiele et al. (2011). We found that the XMM-Newton catalog contained sources that were not in our initial sample. We obtained lightcurves for each of those sources, and any that were significantly detected in our observations were added to the source list.

We determined the position of each source from a merged 0.3–7 keV ACIS image, using the IRAF tool IM-CENTROID. This merged image is registered to the B band image of M31 Field 5 in the Local Group Survey of Massey et al. (2006) using 27 X-ray-bright globular clusters, as described in Barnard et al. (2012a). For transients that were more recent than the merged Chandra image, we registered the Chandra observation with the highest X-ray flux for that transient to the merged Chandra image. For most sources, the position uncertainties combine the systematic uncertainty in registering the merged Chandra image to the Field 5 B band image, and the statistical uncertainty in the position of the X-ray centroid; new transients have an additional uncertainty in registering the peak observation to the merged image.

We obtained 0.3–7.0 keV spectra from circular source and background regions for each source. The background region was the same size as the source region, and at a similar off-axis angle. The extraction radius varied between sources, because larger off-axis angles resulted in larger point spread functions.

2.1. Converting from intensity to luminosity

We used XSPEC to convert from 0.3–7.0 keV intensity to 0.3–10 keV luminosity for each observation of every source. Rather than assuming a single conversion factor for a particular emission model, we calculated the conversion factor at the location of each X-ray source in every observation; this was necessary because any given source could be observed in several different parts of the detector, at various off-axis angles, as the roll angle changed between observations.

We expect most of our X-ray sources to be XBs or

AGN; furthermore, most of the XBs are likely to be in the “hard state” common to all XBs (van der Klis 1994) at luminosities $\lesssim 10\%$ Eddington (Gladstone et al. 2007; Tang et al. 2011). The emission spectra of such sources may be estimated by a power law with photon index (Γ) of 1.7, hence we initially assumed an absorbed power law model for most X-ray sources, with $\Gamma = 1.7$ and line-of-sight absorption (N_{H}) equivalent to 7×10^{20} atom cm^{-2} , the Galactic column density in the direction of M31 (Stark et al. 1992). However, stars and supersoft sources were modeled by 0.05 keV black body spectra with $N_{\text{H}} = 7 \times 10^{20}$ atom cm^{-2} .

2.1.1. ACIS

For ACIS observations, we obtained the response matrices and ancillary response files corresponding to each source spectrum. Net source spectra with >200 photons were freely fitted, starting with the assumed spectra, but with N_{H} and Γ free to vary; if the best fit N_{H} was $< 7 \times 10^{20}$ atom cm^{-2} , then we fixed N_{H} to 7×10^{20} atom cm^{-2} . If an X-ray source exhibited spectra with >200 net counts in only one observation, then we obtained a new lightcurve assuming the best fit model for that observation. If a source had >200 source counts in more than one spectrum, then we plotted N_{H} and Γ (or kT) vs. time, and found the best fit line of constant parameter (N_{H} , Γ or kT), then converted from intensity to flux using these best fit values for observations with <200 net counts.

For transient X-ray sources, we tried two emission models: a power law representing the hard state, and a disk blackbody representing the black hole high state that is often observed in black hole transients during outburst (Remillard & McClintock 2006). If the disk blackbody model was more successful, then we only applied this model to the outburst.

We took this approach because it is unfeasible to fit the individual spectra simultaneously, or create merged spectra for each source. Creating merged spectra is particularly bad, because it involves merging data taken from different parts of the detector, and at different off-axis angles, making the ancillary response extremely complicated and unreliable. However, simultaneous fitting of the individual observations is also unreliable for sources that vary in luminosity or spectral shape, especially if those observations have poor statistics.

2.1.2. HRC

For HRC observations, we included only PI channels 48–293, thereby reducing the instrumental background. We used the WebPIMMS tool to find the unabsorbed luminosity equivalent to 1 count s^{-1} on-axis, assuming the same emission model as for the ACIS observations with <200 photons. We created a 1 keV exposure map for each observation, and compared the exposure within the source region with that of an equivalent on-axis region, in order to estimate the necessary exposure. We multiplied the background subtracted, corrected source intensity by the resulting conversion factor to get the 0.3–10 keV luminosity.

2.1.3. Creating the lightcurves

We created long term 0.3–10 keV lightcurves for each source, using the luminosities obtained from each observation as described above. We only included observations with net source counts ≥ 0 after background subtraction. We fitted each long term lightcurve with a line of constant intensity, in order to ascertain source variability.

We also made 0.5–4.5 keV flux lightcurves for each source that allowed us to make SFs that were directly comparable with the ensemble AGN SF constructed by Vagnetti et al. (2011). We calculated the 0.5–4.5 keV fluxes using the best fit emission model where possible; if no spectral fits were made for a source, then we assumed a typical spectrum with $N_{\text{H}} = 7 \times 10^{20}$ atom cm^{-2} , and a power law with spectral index 1.7.

We note that the structure function for each source is expected to be rather insensitive to the emission model used to convert from intensity to flux. This conversion is a scaling factor that is applied to the intensity lightcurve after correcting for instrumental effects; hence, the emission model is only important if the parameters significantly change between observations.

2.2. Characteristics of the structure function

In this work, we compare the SFs of our X-ray sources with the ensemble AGN SF derived from the XMM-Newton data by Vagnetti et al. (2011): $\text{SF}(\tau) \propto \tau^{0.10 \pm 0.01}$. We estimated the normalization of this relation to be 0.11 from Figure 5 of Vagnetti et al. (2011). Therefore the 3σ upper limit to the AGN SF derived from the XMM-Newton data is given by $0.11\tau^{0.13}$.

Vagnetti et al. (2011) calculated the noise component from

$$\sigma_n^2 = 2 \left\langle (\sigma \log f_X)^2 \right\rangle \simeq 2 (\log e)^2 \left\langle \left(\frac{\sigma f_X}{f_X} \right)^2 \right\rangle, \quad (2)$$

assuming that $\sigma f_X / f_X = (1/N_{\text{phot}})^{0.5}$, and N_{phot} is the number of photons. This assumes that all of the noise in the SF comes from Poisson statistics.

Our lightcurves are background subtracted, and ARF-corrected; furthermore, uncertainties in the luminosities of bright sources include uncertainties in the spectral parameters. As a result, our uncertainties are not simply due to photon counting noise, and may be considerably larger. Hence in our case,

$$\sigma_n^2 \simeq (\log e)^2 \left\langle \left[\frac{\sigma f_X(t+\tau)}{f_X(t+\tau)} \right]^2 + \left[\frac{\sigma f_X(t)}{f_X(t)} \right]^2 \right\rangle, \quad (3)$$

where σf_X is uncertainty in X-ray flux of a particular observation. The simplest possible SF comes from a single pair of observations with X-ray fluxes f_1 and f_2 ; in this case,

$$\sigma_n^2 \simeq (\log e)^2 \left[\left(\frac{\sigma f_1}{f_1} \right)^2 + \left(\frac{\sigma f_2}{f_2} \right)^2 \right]. \quad (4)$$

A constant X-ray source will yield a SF consistent with zero in all τ channels. However, if the variation is smaller than the uncertainty in a given channel, then the SF is imaginary for that channel. Our SFs show imaginary channels with zero power but finite uncertainties; channels that contain no observation pairs have zero power and zero uncertainties.

For each source, we calculated the probability, P_{AGN} , that it was consistent with being a typical AGN like the ones studied by Vagnetti et al. (2011). This was derived from E_i , the excess in channel i over the 3σ limit to the AGN SF observed with XMM-Newton ($0.11\tau^{0.13}$); each SF contained 19 τ channels.

$$P_{\text{AGN}} = \prod_{i=1}^{19} p_i, \quad (5)$$

where $p_i = 1$ when $E_i \leq 0$, and

$$p_i = 1 - \frac{2}{\sqrt{\pi}} \int_0^{E_i/\sqrt{2}} e^{-t^2} dt \equiv \text{erfc}\left(E_i/\sqrt{2}\right) \quad (6)$$

when $E_i > 0$. We then assigned a Rank to each source, given by $-\log(P_{\text{AGN}})$. A Rank of 2.6 indicates a 3σ excess in SF(τ) over $0.11\tau^{0.13}$, while a Rank of 6.2 indicates a 5σ excess.

3. RESULTS

3.1. Overview

We will first provide an overview of our results before dealing with specific aspects of our data. Table 1 summarizes our main results. For each source, we give its position with respect to the LGS M31 Field 5 B band image provided by Massey et al. (2006), along with 1σ position uncertainties. Sources marked with ^a have locations derived from XMM-Newton observations, and 1σ uncertainties calculated from the 3σ uncertainties quoted by Stiele et al. (2011). Sources marked with ^b have positions derived from a highly binned image, where one image pixel is equivalent to 9×9 native pixels. We then show the number of ACIS and HRC observations that contain the source.

Next in Table 1 we present the published source classification and properties. We first show the classification in the Stiele et al. (2011) XMM-Newton catalog of M31 X-ray sources; sources can be classified as XBs (XB), globular clusters (GC), stars (*), galaxies (Gal), AGN (AGN), supernova remnants (SNR), supersoft sources (SSS), or simply hard (H); square brackets indicate candidates, while exclamation marks indicate classifications that were rejected for our Chandra locations. The remaining X-ray sources either were observed but not classified (NC), or had no entry at all (NE). Any improvement on the Stiele et al. (2011) classification is indicated by "="; these can be known X-ray sources that do not appear in the XMM-Newton catalog (X), black hole candidates (BHC), transients (T), novae (Nova), ultra-luminous X-ray sources (U, exhibiting X-ray luminosities $> 2 \times 10^{39}$ erg s⁻¹ Kaur et al. 2012; Noorae et al. 2012; Middleton et al. 2013; Barnard et al. 2013b), or variable stars (var*).

Finally in Table 1 we show the best fit constant 0.3–10 keV luminosity over our ~ 13 year monitoring program, along with the corresponding χ^2/dof , and our ranking of the object according to the variability shown in its structure function. Sources with Rank > 2.6 are significantly more variable than expected for typical AGN. For 28 sources indicated with ^c, we ignored the HRC observations completely; for 120 sources indicated with ^d, we included HRC observations in the luminosity calculation but exclude HRC data from the SF; reasons for these

decisions are given below. The 10 sources indicated with ^e are very soft, and were modelled using an absorbed blackbody with $N_{\text{H}} = 7 \times 10^{20}$ atom cm⁻² and $kT = 0.05$ keV; using our standard emission model for these sources resulted in large systematic offsets between ACIS and HRC luminosities. Likely X-ray binaries are indicated by ^f, while ^g indicates sources that are consistent with AGN.

Our luminosities assume a distance of 780 kpc (Stanek & Garnavich 1998); clearly the distances to foreground stars and background AGN will be very different, along with their corresponding luminosities. In each case, the flux is given by the luminosity divided by 7.3×10^{49} cm².

The following sections describe our source list, spectral analysis, and time variability studies in detail.

3.2. The source list

We initially identified 407 X-ray sources from our Chandra observations; registering the merged 0.3–7 keV image to the LGS B Band optical image resulted in 1σ positional uncertainties of $0.11''$ in RA and $0.09''$ in Dec. Each X-ray source also has an uncertainty in its location on the X-ray image, which is dependent on the source intensity and off-axis angle.

We compared our X-ray sources with the M31 XMM-Newton source catalog of Stiele et al. (2011), by looking for matches within $10''$ of our Chandra positions; these associations were then accepted or rejected based on the 3σ uncertainties in XMM-Newton position reported by Stiele et al. (2011). The XMM-Newton catalog of Stiele et al. (2011) contained ~ 170 X-ray sources that were not in our catalog. We extracted lightcurves and spectra from regions at the positions of these sources, and found evidence for a further 121 X-ray sources; we found no trace of ~ 50 of the X-ray sources in the Stiele et al. (2011). We obtained the positions and uncertainties for the 121 new X-ray sources from Stiele et al. (2011); our total source list contains 528 X-ray sources.

We found that 208 of our X-ray sources had no counterpart in the XMM-Newton catalog despite both catalogs having similar luminosity limits ($\gtrsim 10^{35}$ erg s⁻¹). While 36 of these sources are transient, the remainder were likely missed by XMM-Newton because of its larger PSF and higher background. A further 169 X-ray sources were classified only as ‘‘Hard’’ in Stiele et al. (2011), while another 9 X-ray sources were detected but not classified. Identified sources included 38 GCs or GC candidates; 15 AGN or candidates, including 2 optically identified AGN; 4 novae or candidates; 13 supernova remnants or candidates; 28 foreground stars or candidates; 21 SSS candidates; and 27 XBs or XB candidates including 5 BHCs and 13 transients (Stiele et al. 2011).

We rejected 4 AGN, 2 GC and 3 SN candidates identified in the Stiele et al. (2011) after obtaining our superior Chandra positions. Our total inventory includes 47 foreground stars or candidates; 7 novae or nova candidates; 13 supernova remnants or candidates; and 13 supersoft source candidates with no further classification. Also included are 47 GCs or GC candidates; 36 black hole candidates (12 in GCs), with 1 GC BHC new to this work; and 52 transients (6 located in GCs).

We estimated the probable number of false associations by finding the number of matches between our X-ray

Table 1

Summary of our findings for the 528 X-ray sources in our survey. For each object, we provide its position with respect to the LGS M31 Field 5 B band image provided by Massey et al. (2006), along with 1σ uncertainties in RA and Dec. We then give the number of ACIS and HRC observations, O_A and O_H respectively. Next we show the known properties— first, we give the classification assigned by Stiele et al. (2011), with any further classification following an equals sign. This is followed by the best fit constant luminosity to the unabsorbed 0.3–10 keV luminosity lightcurve and corresponding χ^2/dof . Finally we rank the structure function for variability.

Src	Pos	$\sigma_{\text{RA}}/''$	$\sigma_{\text{Dec}}/''$	O_A	O_H	Properties	$L_{\text{con}}/10^{37}$	χ^2/dof	SF Rank
1	00:41:05.41 +41:18:14.7 ^a	1.3 ^a	1.3 ^a	11	8	H	0.11±0.03	13/18	7.3 ^f
2	00:41:05.46 +41:17:34.1 ^a	1.0 ^a	1.0 ^a	16	11	H	0.062±0.019	22/26	0.5 ^g
3	00:41:07.92 +41:13:44.3 ^a	0.8 ^a	0.8 ^a	21	12	H	0.084±0.019 ^d	36/32	0.9 ^g
4	00:41:09.15 +41:15:17.9 ^a	1.2 ^a	1.2 ^a	20	17	H	0.063±0.016	16/36	0.2 ^g
5	00:41:10.73 +41:21:20.0 ^a	0.9 ^a	0.9 ^a	12	20	[*]=*	0.11±0.02	219/31	51.5
6	00:41:11.40 +41:20:05.6 ^a	0.9 ^a	0.9 ^a	13	12	[*]	0.09±0.02 ^d	8/24	0.0
7	00:41:11.83 +41:23:43.6 ^a	1.4 ^a	1.4 ^a	9	9	H	0.10±0.03	10/17	0.0 ^g
8	00:41:12.42 +41:14:57.6 ^a	0.8 ^a	0.8 ^a	19	25	H	0.139±0.017	59/43	2.6 ^f
9	00:41:13.96 +41:14:34.5 ^a	1.2 ^a	1.2 ^a	22	26	H	0.105±0.016 ^d	55/47	1.4 ^g
10	00:41:14.48 +41:14:00.2 ^a	1.1 ^a	1.1 ^a	20	27	[*]	0.081±0.015	43/46	0.5
11	00:41:15.77 +41:23:28.5 ^a	1.9 ^a	1.9 ^a	10	17	[*]=*	0.08±0.02 ^e	208/26	7.3
12	00:41:17.49 +41:17:26.3 ^a	0.9 ^a	0.9 ^a	22	26	H	0.078±0.016 ^d	34/47	0.2 ^g
13	00:41:17.74 +41:12:55.9 ^a	1.0 ^a	1.0 ^a	24	18	H	0.077±0.015	23/41	1.0 ^g
14	00:41:18.09 +41:10:21.7 ^a	1.0 ^a	1.0 ^a	22	16	H	0.081±0.018 ^c	11/21	0.0 ^g
15	00:41:18.92 +41:08:28.0	1.2	1.1	1	9	H	0.08±0.04	9/9	4.7 ^f
16	00:41:18.98 +41:09:07.6 ^a	1.3 ^a	1.3 ^a	12	6	H	0.06±0.02	14/17	0.0 ^g
17	00:41:20.99 +41:16:01.2 ^a	1.3 ^a	1.3 ^a	19	31	H	0.074±0.015 ^d	21/49	0.0 ^g
18	00:41:21.70 +41:07:55.9 ^b	0.8	0.9	20	4	NC	0.066±0.014	10/23	0.0 ^g
19	00:41:22.62 +41:21:35.3 ^a	1.0 ^a	1.0 ^a	18	45	H	0.139±0.019 ^c	12/17	0.0 ^g
20	00:41:23.25 +41:28:56.9 ^a	1.0 ^a	1.0 ^a	4	8	H	0.16±0.05	8/11	0.1 ^g
21	00:41:23.98 +41:15:09.5 ^a	0.9 ^a	0.9 ^a	20	32	[*]	0.095±0.016 ^d	37/51	0.0
22	00:41:24.9 +41:17:09 ^a	3 ^a	3 ^a	22	33	NC	0.084±0.015 ^d	45/54	0.0 ^g
23	00:41:25.18 +41:19:44.6 ^a	1.1 ^a	1.1 ^a	16	35	*	0.080±0.018	43/50	0.0
24	00:41:25.91 +41:12:59.3 ^a	1.2 ^a	1.2 ^a	19	30	H	0.084±0.016 ^d	34/48	0.0 ^g
25	00:41:27.22 +41:20:03.3 ^a	1.1 ^a	1.1 ^a	18	39	H	0.072±0.015 ^d	39/56	0.4 ^g
26	00:41:29.3 +41:10:41 ^a	2 ^a	2 ^a	18	32	[*]	0.080±0.018 ^d	59/49	0.0
27	00:41:29.72 +41:27:44.4 ^a	1.9 ^a	1.9 ^a	8	8	[*]	0.07±0.02 ^d	5/15	1.0
28	00:41:30.28 +41:28:37.7 ^a	1.1 ^a	1.1 ^a	6	10	[*]	0.05±0.03 ^d	19/15	0.0
29	00:41:31.17 +41:05:03.0	0.8	0.9	16	14	NE	0.058±0.012	173/29	0.0 ^g
30	00:41:31.72 +41:15:21.8 ^a	1.1 ^a	1.1 ^a	26	39	H	0.118±0.016 ^d	53/64	0.5 ^g
31	00:41:31.95 +41:17:46.3 ^a	0.7 ^a	0.7 ^a	28	42	H	0.30±0.02	69/69	3.4 ^f
32	00:41:34.25 +41:17:45.2 ^a	1.6 ^a	1.6 ^a	24	34	H	0.112±0.015	52/57	0.0 ^g
33	00:41:35.74 +41:06:56.3	0.8	1.0	25	20	SNR	0.066±0.010	34/44	0.0
34	00:41:36.08 +41:17:43.0 ^a	1.7 ^a	1.7 ^a	20	37	H=[*],*	0.110±0.013 ^d	39/56	0.0
35	00:41:36.24 +41:12:24.4 ^a	1.5 ^a	1.5 ^a	26	35	H	0.086±0.017	46/60	0.0 ^g
36	00:41:40.13 +41:10:34.9 ^a	1.6 ^a	1.6 ^a	18	35	H	0.106±0.017 ^d	42/52	0.0 ^g
37	00:41:40.15 +41:02:46.9	1.5	1.3	17	11	NE=X	0.038±0.010	16/27	0.1 ^g
38	00:41:41.30 +41:03:33.1	0.8	1.1	26	13	[AGN]	0.118±0.015	43/38	3.5 ^f
39	00:41:41.45 +41:19:15.6 ^a	0.7 ^a	0.7 ^a	19	46	!AGN	0.42±0.02 ^d	93/64	10.4 ^f
40	00:41:41.69 +41:19:54.1 ^a	0.9 ^a	0.9 ^a	16	33	H	0.162±0.015	36/48	0.0 ^g
41	00:41:43.48 +41:05:04.7	0.9	0.8	21	47	*	0.079±0.012 ^e	552/67	16.8
42	00:41:43.51 +41:21:18.2 ^a	0.6 ^a	0.6 ^a	9	32	[XB]	0.112±0.019	46/40	3.7 ^f
43	00:41:44.72 +41:11:09.5	0.5	0.6	30	54	NE	2.04±0.06	2914/83	43.6 ^f
44	00:41:45.34 +41:26:24.1 ^a	0.7 ^a	0.7 ^a	16	56	[AGN]	0.352±0.018	368/71	11.2 ^f
45	00:41:46.76 +41:16:56 ^a	2 ^a	2 ^a	25	36	[AGN]	0.074±0.013 ^d	44/60	0.0 ^g
46	00:41:46.96 +41:23:16.7 ^a	1.5 ^a	1.5 ^a	15	39	H	0.080±0.014	50/53	0.4 ^g
47	00:41:47.55 +41:14:24.9 ^a	1.7 ^a	1.7 ^a	16	34	H	0.089±0.015 ^d	22/49	0.0 ^g
48	00:41:48.23 +41:07:07.9	1.0	1.0	22	31	H	0.060±0.011	29/52	2.2 ^g
49	00:41:49.60 +41:03:33.5	1.0	0.8	14	16	NE	0.08±0.03	20/29	0.0 ^g
50	00:41:49.75 +41:01:07.4 ^b	1.9	1.7	21	17	H	0.65±0.03	396/37	65.3 ^f
51	00:41:50.28 +41:13:35.7	0.8	0.6	20	53	[AGN]	0.272±0.016 ^d	86/72	1.2 ^g
52	00:41:50.43 +41:12:10.4	0.9	1.0	28	38	GC	0.166±0.014	53/65	0.0 ^f
53	00:41:50.71 +41:21:14.3	0.5	0.8	24	47	H	0.163±0.011	54/70	0.0 ^g
54	00:41:51.00 +41:06:48.9 ^a	1.4 ^a	1.4 ^a	21	41	H	0.099±0.016	52/61	0.3 ^g
55	00:41:51.66 +41:14:39.1	0.4	0.4	29	58	!AGN	0.54±0.02	121/86	6.8 ^f
56	00:41:51.86 +41:15:17.1 ^a	1.6 ^a	1.6 ^a	27	33	[*]	0.073±0.013	51/59	2.1
57	00:41:54.31 +41:07:23.2 ^a	0.7 ^a	0.7 ^a	18	38	[SSS]=[Nova]	0.083±0.017 ^d	35/55	0.0
58	00:41:54.83 +41:07:34.3	0.6	1.1	20	32	H	0.134±0.019	38/51	0.0 ^g
59	00:41:55.24 +41:23:01.8	0.8	0.8	16	48	H	0.105±0.009 ^d	107/63	27.1 ^f
60	00:41:57.24 +41:14:40.2 ^a	1.5 ^a	1.5 ^a	41	29	H	0.053±0.011 ^d	38/69	0.0 ^g

^a Positions and uncertainties obtained from Stiele et al. (2011); ^b position uncertainty obtained from a 9×9 binned image; ^c HRC observations ignored; ^d HRC observations included in luminosity fit but not SF; ^e fitted with blackbody model $N_H = 7 \times 10^{20}$ atom cm^{-2} , $kT = 0.05$ keV; ^f likely XB; ^g consistent with AGN.

sources and astronomical objects after adding $20''$ to or subtracting $20''$ from the Right Ascension or Declination. In each of the four tests we found 6–11 false matches with stars, 0–1 false matches with a candidate supernova remnant, 0–2 false matches with candidate globular clusters, and 1–4 false matches with novae.

3.3. Spectral fitting

We found 120 sources that had spectra with >200 net source counts in at least one ACIS observation. We fitted the spectra with the emission model that suited the source classification; stars were fitted with blackbody models, X-ray transients in outburst were fitted with disk blackbody models (see e.g. Barnard et al. 2012a), and the remaining sources were fitted with power law models; each model included line-of-sight absorption, with a minimum value equivalent to 7×10^{20} H atom cm^{-2} .

High quality XMM-Newton observations of the brightest sources in our survey required two-component models (e.g. blackbody + power law, see Barnard et al. 2006, for an example); however, Chandra spectra from these sources were acceptably fitted by simple power laws ($\Gamma \lesssim 1$). Due to the difference between HRC and ACIS responses, we ignored the HRC data for these systems; even if we used two component emission models, it would be impossible to estimate the HRC luminosities due to the uncertainties in the contributions of the different components.

For sources with multiple spectral fits, we obtained the best fit constant values for the absorption and emission parameter, along with the corresponding χ^2/dof , where the dof is one less than the number of fitted observations. Table 2 summarizes our findings. For each source we provide the emission model used (power law “PO”, blackbody “BB”, or disk blackbody “DBB”), absorption ($N_{\text{H}}/10^{22}$ atom cm^{-2}) plus χ^2/dof , and parameter (photon index for PO, kT/keV for BB or DBB) plus χ^2/dof . If only one observation was fitted, then the χ^2/dof is given as —; in cases with only 2 observations (1 degree of freedom), χ^2 was often extremely low, and meaningless. The absorption was fixed to Galactic line of sight absorption (7×10^{20} atom cm^{-2}) for three sources (S175, S250, and S287).

In many cases, the parameter fits have low χ^2/dof ; this is to be expected when each datum is itself derived from fitting a spectrum which may have large uncertainties. Only one source (S327) exhibited significant variation in absorption. Five sources (S117, S209, S251, S327, and S396) exhibited significant variability in their emission parameters; indeed the variability in S209 was so extreme that the HRC observations were unusable (each ACIS observation had sufficient counts for fitting). S117, S251 and S396 are transients, S209 is a candidate Z-source (Barnard et al. 2003), and S327 is a black hole candidate (Barnard et al. 2013a). It is unsurprising that so few X-ray sources exhibited spectral variability, since the hard state is observed up to ~ 0.1 times the Eddington limit ($\sim 2 \times 10^{37}$ erg s^{-1} for a $1.4 M_{\odot}$ NS), and $\sim 90\%$ of our sample is consistent with being in the NS hard state. For example, S213 has a best fit luminosity $\sim 10^{37}$ erg s^{-1} and a Rank >320 , and the entire 0.3–10 keV lightcurve is consistent with S213 being in a NS hard state. Furthermore, the statistics led to relatively large uncertainties

in the emission parameters, making significant variability harder to detect than for Galactic XBs.

3.4. X-ray identification of foreground stars

Many foreground stars, or candidates, were identified by their proximity to an optical counterpart. Some of these stars were identified as Hard by (Stiele et al. 2011), due to overlapping selection criteria ($\text{HR2-EHR2} > -0.2$ for hard sources with no other classification, but $\text{HR2-EHR2} < 0.3$ for foreground stars along with other criteria). We label these sources as “H=[*]”.

It was therefore necessary to investigate these sources further, using the best ACIS spectra available; if the observed counts fell mostly below 1 keV, then we considered the source a foreground star, indicated by “H=[*],*”. Otherwise we considered them a “hard” source, “H=[*],H”. If there were too few counts to even determine this much, then we conservatively classify the source as a candidate star, “H=[*],[*]”. Two sources (S34, and S74) were classified as stars, and four sources (S138, S165, S282, S402) were classified as candidate stars. Seven sources (S87, S92, S340, S399, S405, S499, and S507) were classified as hard.

3.5. Long-term variability

We assessed the long-term variability of each X-ray source in two ways: the 0.3–10 keV lightcurves, and the 0.5–4.5 keV SFs. The instrumental responses of the ACIS and HRC instruments are significantly different, and the only the ACIS observations are capable of providing reliable spectral data. Therefore, we made two lightcurves and two SFs for each source, one including ACIS and HRC observations, and one including only ACIS data.

There are two situations in which the inclusion of HRC data may be detrimental to our studies of a particular X-ray source. In the first situation, where the HRC lightcurve is systematically offset from the ACIS lightcurve due to differences in instrumental response, we exclude the HRC observations entirely; such cases are indicated by ^c in Table 1. In the second situation, where particularly large uncertainties in HRC observations dominate the structure functions, we include the HRC observations in our luminosity estimates, but exclude them from our SFs; these cases are indicated by ^d in Table 1. Whenever the two SFs for a particular source gave conflicting results, we favored the ACIS-only SF.

The first situation can affect any source, but is particularly important for bright sources exhibiting significant spectral evolution. The ACIS and HRC luminosities only agree if the chosen emission model is appropriate for the observed spectrum. For most sources, we must assume a standard spectrum; this is successful in many cases, but for those that are unsuccessful, using only the ACIS data minimizes the uncertainties in luminosity and variability.

The second situation affects some faint X-ray sources. Some HRC observations have exposure times as short as 1 ks; since the sensitivity of the HRC is a factor ~ 5 lower than the ACIS for typical X-ray binary spectra, the large uncertainties in HRC luminosities can dominate the SF to the extent that variability between ACIS observations is lost.

The 0.5–10 keV flux distribution obtained by Georgakakis et al. (2008) leads us to expect 635 AGN

Table 2
Spectral fits for sources with >200 net source counts in at least one ACIS observation.

Src	Model	$N_{\text{H}}/10^{22}$	χ^2/dof	Param	χ^2/dof
31	PO	0.3 ± 0.2	—	2.3 ± 0.9	—
43	PO	0.31 ± 0.04	4/11	2.37 ± 0.11	3/11
55	PO	0.19 ± 0.12	—	2.1 ± 0.4	—
78	PO	0.34 ± 0.04	8/9	1.85 ± 0.07	3/9
83	PO	0.33 ± 0.14	2/3	1.57 ± 0.18	1.1/3
84	PO	0.50 ± 0.13	1.6/5	2.3 ± 0.2	1.4/5
90	PO	0.11 ± 0.07	0.13/2	1.7 ± 0.2	0.31/2
95	PO	0.45 ± 0.09	0.2/3	1.85 ± 0.13	1.4/3
100	BB	0.129 ± 0.019	12/47	0.572 ± 0.007	37/47
103	PO	0.28 ± 0.06	0.13/4	2.12 ± 0.13	4/4
106	PO	0.12 ± 0.12	—	1.7 ± 0.4	—
108	PO	0.41 ± 0.09	1.1/2	2.05 ± 0.18	7/2
109	PO	0.5 ± 0.06	5/17	1.51 ± 0.08	5/17
111	PO	0.6 ± 0.2	0.06/1	1.9 ± 0.3	0.3/1
117	DBB	0.06 ± 0.04	0.006/1	0.38 ± 0.02	14/1
120	PO	0.30 ± 0.04	8/24	2.88 ± 0.12	10/24
122	PO	0.16 ± 0.04	5/15	1.47 ± 0.07	4/15
142	PO	0.41 ± 0.04	9/14	2.16 ± 0.07	8/14
143	PO	0.18 ± 0.09	0.3/1	2.2 ± 0.2	0.002/1
146	PO	0.13 ± 0.13	—	1.2 ± 0.4	—
148	PO	0.14 ± 0.04	4/5	1.74 ± 0.09	6/5
151	PO	0.125 ± 0.009	77/86	1.552 ± 0.015	76/86
153	PO	0.13 ± 0.05	1.9/6	1.79 ± 0.13	1.9/6
158	PO	0.18 ± 0.06	1.2/6	2.2 ± 0.1	4/6
159	PO	0.43 ± 0.05	1.5/9	1.89 ± 0.07	6/9
160	PO	0.26 ± 0.12	0.7/4	1.7 ± 0.2	0.4/4
167	PO	0.16 ± 0.04	4/5	1.5 ± 0.1	6/5
168	PO	0.11 ± 0.02	11/37	1.58 ± 0.03	14/37
171	PO	0.1 ± 0.05	2/5	2.05 ± 0.12	3/5
175	BB	$0.07\pm f$	—	0.25 ± 0.03	—
179	PO	0.159 ± 0.012	39/94	1.69 ± 0.03	49/94
181	PO	0.25 ± 0.04	3/8	1.90 ± 0.09	3/8
184	PO	0.068 ± 0.013	11/38	1.25 ± 0.03	23/38
188	PO	0.18 ± 0.07	1.4/6	1.65 ± 0.14	1.1/6
195	PO	0.08 ± 0.03	1.5/8	1.61 ± 0.07	3/8
198	PO	0.15 ± 0.07	1.5/4	1.37 ± 0.15	2/4
201	PO	0.31 ± 0.10	4/9	1.72 ± 0.17	3/8
209	PO	0.073 ± 0.007	45/104	0.856 ± 0.008	370/104
213	PO	0.22 ± 0.05	2/5	2.36 ± 0.16	3/5
214	PO	0.1 ± 0.02	—	1.74 ± 0.09	—
217	PO	0.113 ± 0.014	8/16	1.88 ± 0.04	22/16
219	PO	0.26 ± 0.05	3/9	1.73 ± 0.08	4/9
223	PO	0.1 ± 0.02	6/11	1.64 ± 0.05	10/11
229	PO	0.11 ± 0.05	1.1/5	1.73 ± 0.14	0.3/5
231	PO	0.3 ± 0.30	—	1.5 ± 0.5	—
233	PO	0.3 ± 0.2	0.05/1	2.1 ± 0.4	0.5/1
236	PO	0.09 ± 0.03	1.1/9	1.41 ± 0.07	4/9
238	PO	0.07 ± 0.02	3/10	1.95 ± 0.06	4/9
241	PO	0.12 ± 0.02	5/11	1.44 ± 0.05	6/11
247	PO	0.07 ± 0.02	1.4/10	1.52 ± 0.05	6/10
249	PO	0.5 ± 0.3	—	2.6 ± 0.6	—
250	BB	$0.07\pm f$	—	0.21 ± 0.02	—
251	DBB	0.319 ± 0.010	3/6	0.656 ± 0.007	47/6
252	PO	0.15 ± 0.02	5/10	1.75 ± 0.05	8/10
253	PO	0.12 ± 0.09	1.8/1	2.4 ± 0.3	0.16/2
254	PO	0.20 ± 0.05	3/8	1.78 ± 0.11	3/8
255	PO	0.13 ± 0.04	3/8	1.51 ± 0.08	3/8
256	PO	0.10 ± 0.04	1.6/6	1.52 ± 0.11	3/6
260	PO	0.09 ± 0.04	0.2/4	2.12 ± 0.14	2/4
264	PO	0.08 ± 0.03	0.8/7	2.27 ± 0.12	3/7

within our $20'$ region with fluxes $\gtrsim 1.4 \times 10^{-15}$ erg cm $^{-2}$ s $^{-1}$, equivalent to luminosities $> 10^{35}$ erg s $^{-1}$ at 780 kpc; if the sensitivity of our survey were uniform, we would expect to observe < 2 typical AGN (as defined by Vagnetti et al. 2011) with Rank ≥ 2.6 . Considering the deterioration of sensitivity with off-axis angle, and the fact that our uncertainties in the background-subtracted luminosities are often substantially larger than the Poisson statistics assumed by Vagnetti et al. (2011), we expect $\ll 1$ typical AGN to exhibit Rank ≥ 2.6 .

Since we assume a particular emission model to convert from counts to luminosity in many cases, spectral

variation in the X-ray sources would lead to systematic uncertainties. However, $\sim 90\%$ of our sample exhibited 0.3–10 keV luminosities consistent with the NS hard state throughout our 13 year monitoring campaign, hence we expect little spectral variation from these sources. Furthermore, only 5 out of the 120 X-ray sources with freely fitted spectra exhibited significant spectral variation. Hence spectral change is unlikely to be a major source of systematic uncertainties in estimating luminosity variability.

3.5.1. Classifying the X-ray sources

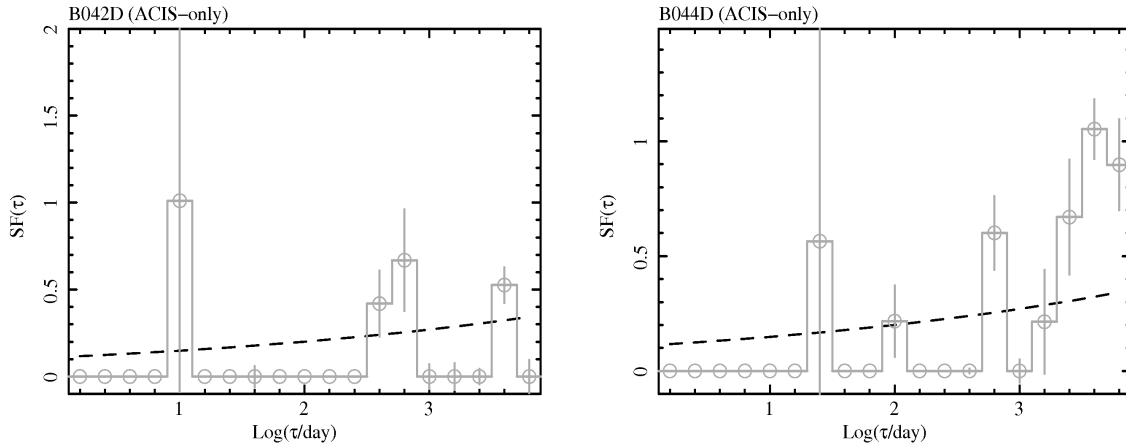


Figure 1. 0.5–4.5 keV ACIS-only SFs for the two AGN associated with optical galaxies, B042D and B044D. The dashed curves represent $SF(\tau) = 0.11\tau^{0.13}$, the 3σ upper limit to the ensemble AGN SF created by Vagnetti et al. (2011) from XMM-Newton data. These galaxies have luminosities $\sim 10^{42}$ and $\sim 10^{41}$ erg s^{-1} respectively, 1–5 orders of magnitude lower than the galaxies in the sample used by Vagnetti et al. (2011).

We found 246 sources with SF Rank ≥ 2.6 , and 282 sources with Rank < 2.6 . Sources with Rank ≥ 2.6 include 18 foreground stars, 5 supersoft sources, 7 supernova remnants, 1 nova, and 2 low-luminosity AGN (discussed below); the supernova remnants are extended, and not expected to be variable, hence we assume that the associations of strongly variable X-ray sources with supernova remnants are coincidental. Sources with Rank < 2.6 include 11 transients, 13 sources associated with GCs, 29 stars, 8 supersoft sources, 6 novae, and 6 bright X-ray binaries.

We classify as X-ray binaries all 52 X-ray transients (this number excludes novae), all 47 globular cluster sources, the 7 variable sources associated with supernova remnants, 144 unclassified X-ray sources with Rank ≥ 2.6 , and 6 bright X-ray binaries with Rank < 2.6 ; we therefore identify 250 X-ray binaries in total (6 transients are located in GCs). We do not count the novae or unidentified supersoft sources, although some of them may be XBs. It is perhaps surprising that 11 transients exhibited Ranks < 2.6 ; however, the lightcurves for these sources include many observations when they were in quiescence, meaning that the noise dominates the SFs for these sources. We found 161 XBs with Rank ≥ 6.4 (a 5σ rejection of the AGN classification), and 36 XBs have Ranks > 320 , the limit imposed by machine precision.

We found that 202 unclassified X-ray sources and 1 Galaxy candidate identified by Stiele et al. (2011) exhibited Ranks < 2.6 , and are consistent with being AGN. In addition there are two optically identified AGN that exhibit high variability: the ACIS-only SF for S73 has Rank 2.6, while the ACIS-only SF for S75 has Rank 12.3 (shown in Figure 1); the ACIS+HRC SFs were dominated by noise from the HRC. However, these galaxies (B042D and B044D) are relatively nearby (with velocities of 57833 km s^{-1} and 35743 km s^{-1} respectively, Caldwell et al. 2009), and exhibited low luminosities ($\sim 10^{42}$ erg s^{-1} and $\sim 10^{41}$ erg s^{-1}). The ensemble AGN SF created by Vagnetti et al. (2011) sampled AGN with luminosities 10^{43} – $10^{45.5}$ erg s^{-1} , ~ 1 – 5 orders of magnitude higher than S73 and S75; therefore we estimated the variability seen at 10^{41} and 10^{42} erg s^{-1} using the published relations between luminosity

and variability: $I_{\text{var}} \propto L^{-0.21}$ over ~ 100 day time-scales (Vagnetti et al. 2011), and $I_{\text{var}} \propto L^{-0.13}$ over year time-scales (Markowitz & Edelson 2004). We found that S73 and S75 were both consistent with the expected AGN SF when scaled to their luminosities. These results do not jeopardize our ranking system, since we expect that other low-luminosity AGN would have to be local to be detected, and that such nearby AGN would be identified in other wavelengths.

Figure 2 compares the long-term lightcurves and SFs of three X-ray sources. Panels a) and b) show the lightcurve and SF for S381, one of the faintest X-ray sources with a Rank > 2.6 . S381 has a mean 0.3–10 keV luminosity of $1.1 \pm 0.3 \times 10^{35}$ erg s^{-1} , with $\chi^2/\text{dof} = 47/49$; its SF yielded a Rank of 11.1. We note that the SF includes several bins with zero SF but finite uncertainties; $SF(\tau)$ is imaginary for these bins, because the variation is smaller than the noise. Panels c) and d) give the ACIS-only lightcurve and SF for S209, one of the brightest X-ray sources in the field of view; $\chi^2/\text{dof} = 1255/106$ for its best fit constant intensity, yet its SF shows less fractional variation than a typical AGN over all time-scales. S209 is one of those sources where the HRC data were excluded entirely from the analysis. Panels e) and f) show the lightcurve and SF for S213, one of the 36 XBs with Rank > 320 . These results agree with the well known behavior of Galactic XBs where the high luminosity XBs only vary by a factor of a few, while low luminosity XBs can vary in intensity by 1–2 orders of magnitude (see e.g. Munro et al. 2002).

In Figure 3 we compare the Rank and luminosity for our sources identified as XBs and possible AGN. We see that sources with Rank < 2.6 are found at 0.3–10 keV luminosities $\lesssim 6 \times 10^{36}$ erg s^{-1} and $\gtrsim 5 \times 10^{37}$ erg s^{-1} ; it is well known that high luminosity XBs in our Galaxy are substantially less variable than low luminosity XBs (Munro et al. 2002). It is possible that the intrinsic variability of some faint XBs was obscured by the scarcity of observed photons. The median Ranks for our XBs, sources consistent with AGN, and the remaining sources are 11.2, 0.0, and 1.0, respectively; clearly our XB population is vastly more variable than the other classes of sources.

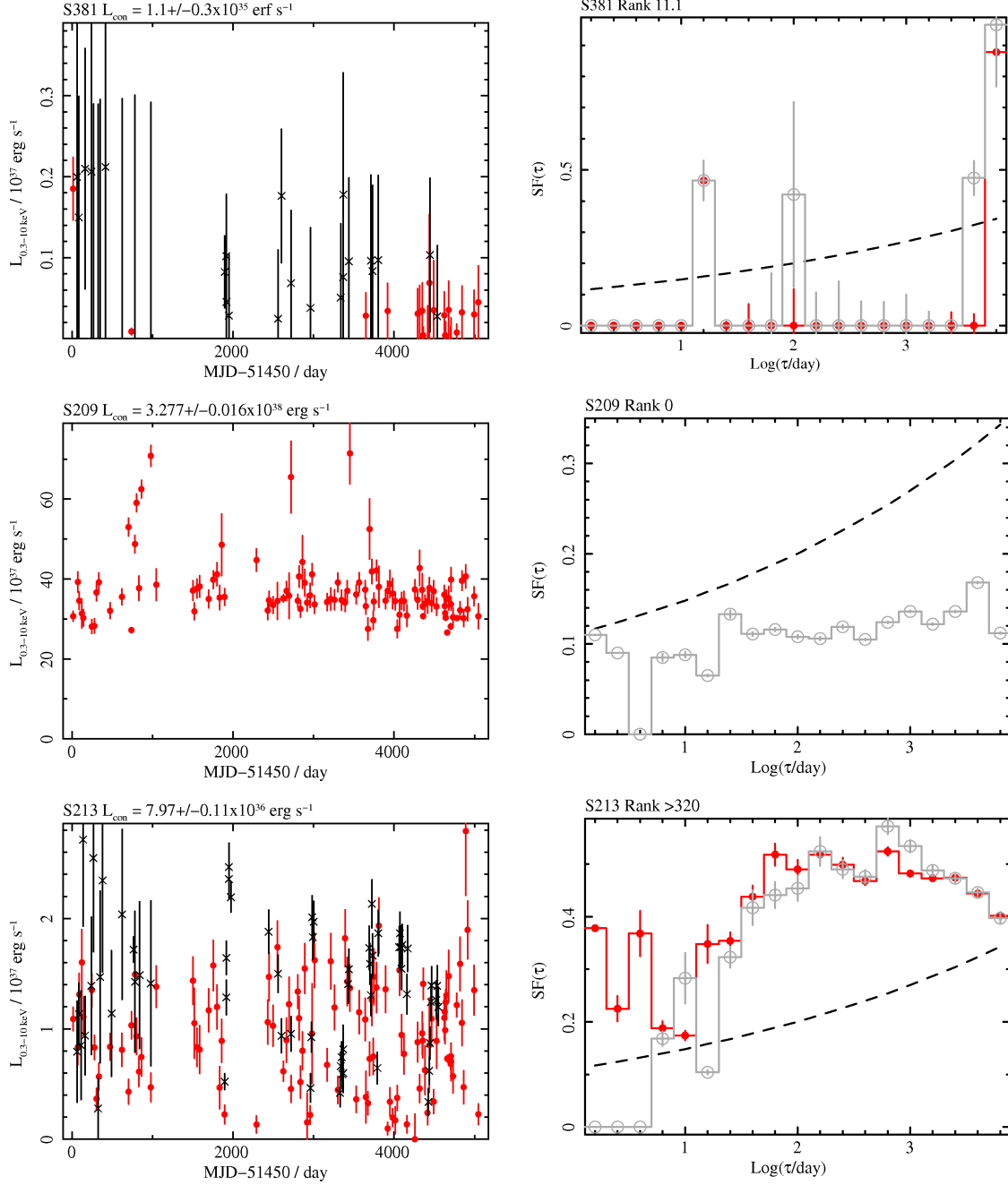


Figure 2. Long-term 0.3–10 keV lightcurves and 0.5–4.5 keV structure functions for three representative X-ray sources. S381 is one of the faintest X-ray binary candidates that we identify from its SF (Rank = 11.1); SF(τ) is imaginary for channels where the variation is less than the noise: this is indicated by zero power and finite uncertainties. S209 is one of our brightest XBs; even though its variability is highly significant, the fractional variation is lower than expected for typical AGN. S213 is representative of our low luminosity XBs with a SF that clearly distinguishes it from an AGN; its Rank is >320 . In each lightcurve, ACIS and HRC observations are represented by circles and crosses respectively; no HRC data was used for S209. For the SFs, closed circles represent SFS from the ACIS and HRC observations, while open circles represent the ACIS-only SFs; dashed lines represent $\text{SF}(\tau) = 0.11\tau^{0.13}$.

3.5.2. Comparing our possible AGN population with expected AGN

We found 205 X-ray sources to be consistent with AGN; however, this sample may contain some faint XBs. Georgakakis et al. (2008) have created a flux distribution (i.e. $\log N$ vs $\log S$) for AGN in the 0.5–10 keV band, which is similar enough to our 0.3–10 keV band for comparison; the 0.3–10 keV and 0.5–10 keV fluxes for our possible AGN agree to within $\sim 10\%$. If we simply scale

this distribution to a circular area with $20'$ radius, then we expect 635 AGN with fluxes $> 1.4 \times 10^{-15} \text{ erg cm}^{-2}$ (equivalent to luminosities $> 10^{35} \text{ erg s}^{-1}$ for sources in M31); this is a factor ~ 3 times greater than the number of observed AGN candidates, and more than total of observed X-ray sources. The origin of this discrepancy could be astronomical, if absorbing material in the M31 bulge reduces the observed number of faint AGN. Alternatively, this effect could be instrumental, since the sensitivity of the Chandra τ images is reduced at large off-

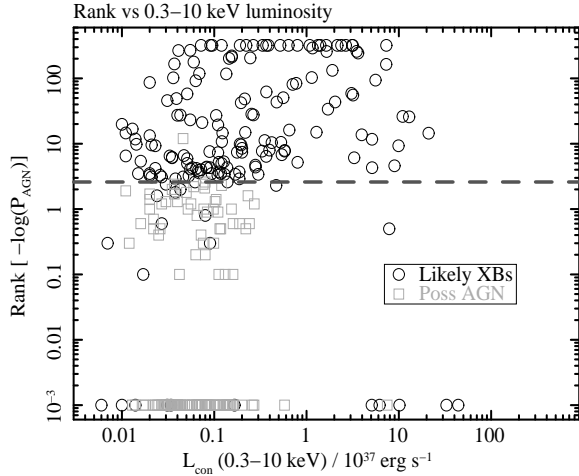


Figure 3. Comparison of Rank (i.e. $-\log[P_{\text{AGN}}]$) vs. 0.3–10 keV luminosity for our X-ray binaries (open circles) and sources consistent with AGN (open squares). The dashed line indicates a Rank of 2.6, corresponding to a 3σ rejection of an AGN identification. An offset of 0.001 was added to those sources with Rank 0, to allow them to show up on a log scale.

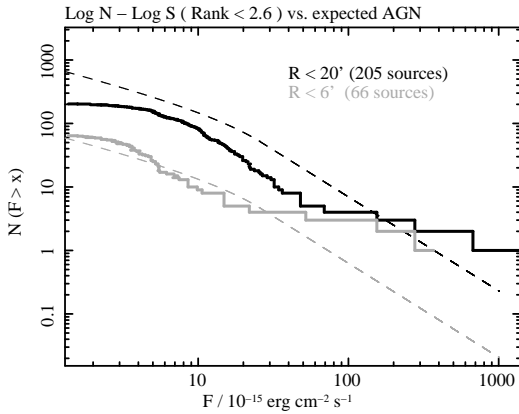


Figure 4. Comparison between the 0.3–10 keV flux distribution of observed AGN candidates (solid lines) and the expected 0.5–10 keV AGN distribution from Georgakakis et al. (2008) (dashed lines). The 0.3–10 keV and 0.5–10 keV fluxes agree to within 10%. Black and gray lines correspond to circular regions with 20' and 6' radius, respectively.

axis angles by vignetting and reduced exposure; our normalization of the AGN flux distribution assumes uniform sensitivity.

Therefore, we compared the AGN candidates with the expected AGN within 6' of the M31 nucleus. We expected 56 AGN, and observed 66 AGN candidates within this region. Given that we see an excess of sources consistent with AGN over the expected amount within 6' of M31*, and only $\sim 30\%$ expected sources within 20' of M31*, this deficit is probably dominated by instrumental effects.

We compare the 0.3–10 keV flux distribution of the observed AGN candidates with the expected 0.5–10 keV flux distribution found by Georgakakis et al. (2008) for the two regions (with radius 20' and 6') in Fig. 4. Solid, stepped lines indicate the observed flux distributions, while dashed lines show the expected distributions; black lines correspond to the 20' region, and grey lines to the 6' region. We see that the flux distributions of possi-

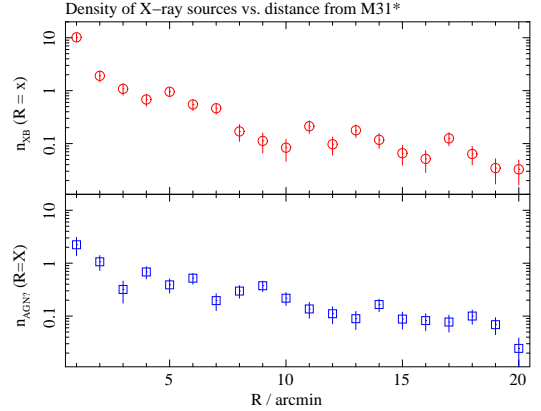


Figure 5. Number densities of our XBs (top) and AGN (bottom) vs. distance from galactic center (in the plane of the detector). We expect XB density to follow stellar mass, while AGN density is expected to be constant.

ble AGN are considerably flatter than expected; together with the excess seen in the population within 6', these results suggest that some of the sources with Rank < 2.6 are unidentified XBs.

3.6. Number density of XBs and AGN vs distance from M31*

We calculated the number densities of our 250 XBs and our 203 possible AGN per arcmin² vs. distance from M31* in the detector plane. We present our findings in Fig. 5.

Our variability survey makes no distinction between low mass X-ray binaries (LMXBs) and high mass X-ray binaries (HMXBs). LMXBs are old, and their numbers tend to follow stellar mass; HMXBs are young, and their populations depend on the star formation rate (see e.g. Grimm et al. 2003). A proper comparison between the distribution of our XBs and the expected distribution is beyond the scope of this paper. However, the observed distribution does appear to agree with expectations (c.f. Fig. 9 of Voss & Gilfanov 2007, taking into account differences in normalization due to different luminosity limits).

We might expect the AGN density to remain constant, with a possible decrease at large distances to account for decreasing instrument sensitivity. However, the number density of possible AGN is considerably higher for regions closer to M31*, again consistent with the presence of some XBs in our sample of possible AGN.

3.7. A newly identified transient black hole candidate in the globular cluster B128

In Barnard et al. (2013a), we identified 26 new black hole candidates (BHCs) in our Chandra observations using a three step process. First we established that the X-ray source was an XB, using SF analysis or by associations with a globular cluster, or by flux. Next we looked for high quality hard state spectra (represented by power law emission with photon index $\Gamma \sim 1.4\text{--}2.1$) at luminosities above the threshold for neutron star (NS) XBs ($\sim 3 \times 10^{37}$ erg s⁻¹). Finally we modelled these spectra with disk blackbody + blackbody emission models, and compared the values with the parameter space defined by soft NS XB spectra (Lin et al. 2007, 2009, 2012).

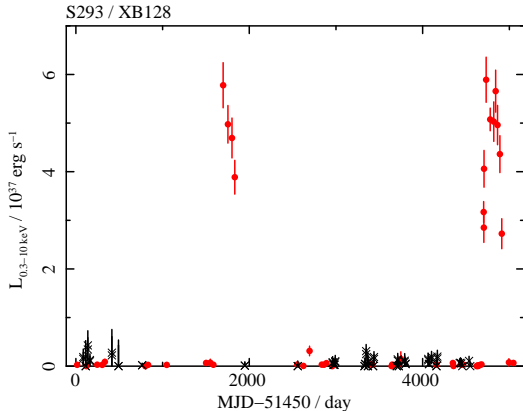


Figure 6. Our long-term 0.3–10 keV luminosity lightcurve for S293 / XB128, a recurrent transient X-ray binary associated with the M31 GC B128 that may contain a black hole. ACIS and HRC observations are represented by circles and crosses respectively.

S293 in our survey is a newly identified BHC associated with the confirmed old M31 GC known as B128, following the Revised Bologna Catalog v 3.4 (Galleti et al. 2004, 2006, 2007, 2009). S293, also known as XB128 following our naming convention for X-ray sources associated with GCs (see e.g. Barnard et al. 2013a), is a transient X-ray source that has exhibited two outbursts during our monitoring campaign. We present a 0.3–10 keV lightcurve of XB128 in Fig. 6.

The first outburst occurred in 2004 May, reaching a 0.3–10 keV luminosity of $5.3 \pm 0.4 \times 10^{37}$ erg s $^{-1}$ and lasted at least 134 days; unfortunately, the nearest observation containing XB128 prior to the burst was 113 days earlier, and the next one was 114 days after the last bright observation. The first outburst was only seen in decline.

We caught the second outburst during the rise in 2012 August, with a maximum 0.3–10 keV luminosity of $5.9 \pm 0.4 \times 10^{37}$ erg s $^{-1}$; the true peak may not have been observed. It was still active 210 days after our first detection of the outburst, but had disappeared the next time that region was observed 62 days later.

During a ~ 40 ks ACIS-S observation (Obs ID 14196), a power law fit to the spectrum of XB128 gave $N_{\text{H}} = 8 \pm 5 \times 10^{20}$ atom cm $^{-2}$ and $\Gamma = 1.54 \pm 0.09$ with $\chi^2/\text{dof} = 56/63$; the 0.3–10 keV luminosity was $5.1 \pm 0.2 \times 10^{37}$ erg s $^{-1}$. This is the best spectrum we have for XB128 that supports a BHC classification, with 1550 net source counts.

We fitted this spectrum with a disk blackbody + blackbody emission model, and found the 2–10 keV luminosities for each component. This is for comparison with the NS XB soft state parameter space that was ascertained from hundreds of RXTE spectra analyzed by Lin et al. (2007, 2009, 2012).

Our criteria for identifying black hole candidates from their disk blackbody + blackbody fits are presented in Barnard et al. (2013a) and summarized as follows. Lin et al. (2007, 2009) were unable to obtain successful fits to hard state spectra with their double thermal (disk blackbody + blackbody) model; the disk blackbody temperature is forced to low values because it must account for the low energy flux, and contributes little to the 2–10 keV flux. By contrast, Lin et al. (2007, 2009, 2012) found the

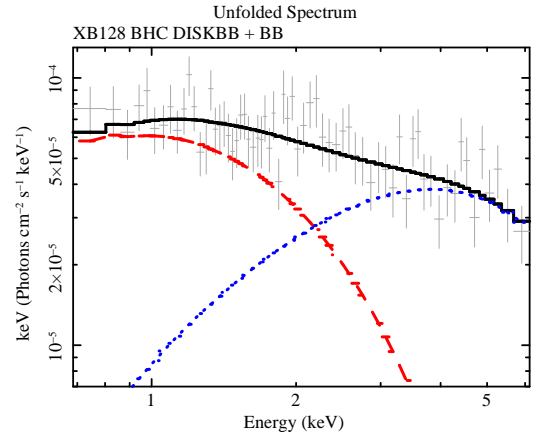


Figure 7. Unfolded spectrum for S293 / XB128 from the ~ 40 ks ACIS-S observation 14196, with the best fit double thermal model. The disk blackbody and blackbody components are represented by dashed and dotted curves respectively. The y-axis is multiplied by channel energy.

the disk blackbody component dominated their bright NS spectra, with temperatures $\gtrsim 1$ keV. Since we identify our BHCs from high luminosity hard states, we expect double thermal fits to BHC spectra to result in low temperatures and small contributions to the 2–10 keV flux from the disk blackbody components (Barnard et al. 2013a).

When fitting the double thermal model, the absorption was fixed to 7×10^{20} atom cm $^{-2}$, equivalent to the Galactic line-of-sight absorption; the absorption was unreasonably low when freely fitted. The disk blackbody contributed $4 \pm 2 \times 10^{36}$ erg s $^{-1}$ to the 2–10 keV luminosity, with an inner disk temperature of $0.59_{-0.11}^{+0.16}$ keV. The blackbody component had a temperature of $1.35_{-0.18}^{+0.4}$ keV, emitting $2.4 \pm 0.2 \times 10^{37}$ erg s $^{-1}$. The total 2–10 keV luminosity was $2.8 \pm 0.3 \times 10^{37}$ erg s $^{-1}$, and $\chi^2/\text{dof} = 57/62$. We present the unfolded spectrum fitted with this model in Fig. 7. The disk blackbody temperature was 2.8σ below 1 keV; furthermore, its 2–10 keV contribution was 3.8σ below 50%. Hence, XB128 is unlikely to contain a NS primary (probability of disk blackbody temperature and contribution being consistent with a NS $\sim 7 \times 10^{-7}$), and is a strong black hole candidate.

Optical spectroscopy of the globular cluster B128 revealed that it has an age $\sim 10^{10.1}$ year, a mass of $\sim 10^{5.32} M_{\odot}$, and metallicity $[\text{Fe}/\text{H}] = -0.56$; it is ranked 68 out of 379 GCs by metallicity ($>82\%$) and ranked 204 ($>46\%$) by mass (Caldwell et al. 2009, 2011). We have previously found 11 GC BHCs, and they are all found in GCs that are significantly more massive, more metal rich, or both, than the general GC population in M31 (Barnard et al. 2008; Barnard & Kolb 2009; Barnard et al. 2011, 2012b, 2013a). The GC B128 continues this trend, being near average mass but particularly metal rich.

4. SUMMARY AND CONCLUSIONS

We have applied a novel technique for distinguishing between XBs and AGN to 528 X-ray sources in the central region of M31, observed ~ 170 times over the last 13 years with Chandra. We identified 250 likely XBs in total; this includes ~ 200 new X-ray binary identifications. Previously, only ~ 50 XBs and ~ 40 XB candidates had

been identified out of ~ 2000 X-ray sources within the D_{25} region of M31 (Stiele et al. 2011).

We find that up to 205 X-ray sources with 0.3–10 keV fluxes $\gtrsim 1.4 \times 10^{-15}$ erg cm $^{-2}$ s $^{-1}$ are consistent with being AGN; this is a factor ~ 3 lower than expected from the 0.5–10 keV flux distribution found by Georgakakis et al. (2008). We find that this difference is due to instrumental effects: simply scaling the Georgakakis et al. (2008) relation by area implies a constant sensitivity, but the Chandra sensitivity significantly decreases with increasing off-axis angle.

Our SF analysis technique for identifying X-ray binaries could be applied to several well-studied nearby galaxies. We find that the low luminosity XBs tend to be significantly more variable than the high luminosity ones (in agreement with observations of Galactic XB behavior Munro et al. 2002); hence this technique is not suitable for distant galaxies where only very luminous XBs are detected.

Furthermore, we identify a new transient black hole candidate, associated with the confirmed globular cluster B128. This X-ray source, known as XB128, exhibited two outbursts during our monitoring observations. We obtained a 40 ks ACIS-S spectrum during the observed peak of the second outburst, and fitted it with a disk blackbody + blackbody emission model for comparison with the full gamut of spectra exhibited by Galactic neutron star binaries and analyzed by Lin et al. (2007, 2009, 2012). The disk blackbody component for XB128 was inconsistent with neutron star spectra at a $> 5\sigma$ level, hence we label it a black hole candidate, following Barnard et al. (2013a).

ACKNOWLEDGMENTS

We thank the anonymous referee, whose thoughtful comments substantially improved this paper. This research has made use of data obtained from the Chandra data archive, and software provided by the Chandra X-ray Center (CXC). This work was supported by Chandra grants GO2-13106X, and GO3-14095X.

Facilities: CXO (ASIS) CXO (HRC).

REFERENCES

- Barnard, R., Church, M. J. & Bałucińska-Church, M. 2003, *A&A*, 405, 237
- Barnard, R., Foulkes, S. B., Haswell, C. A., et al. 2006, *MNRAS*, 366, 287
- Barnard, R., Stiele, H., Hatzidimitriou, D., et al. 2008, *ApJ*, 689, 1215
- Barnard, R. & Kolb, U. 2009, *MNRAS*, 397, L92
- Barnard, R., Garcia, M. R., & Murray, S. S. 2011, *ApJ*, 743, 185
- Barnard, R., Galache, J. L., Garcia, M. R., et al. 2012a, *ApJ*, 756, 32
- Barnard, R., Garcia, M., & Murray, S. S. 2012b, *ApJ*, 757, 40
- Barnard, R., Garcia, M. R., & Murray, S. S. 2013, *ApJ*, 770, 148
- Barnard, R., Garcia, M. R., & Murray, S. S., Primini, F. 2013, *ApJ*, 772, 126
- Caldwell, N., Harding, P., Morrison, H., et al. 2009, *AJ*, 137, 94
- Caldwell, N., Schiavon, R., Morrison, H., Rose, J. A., & Harding, P. 2011, *AJ*, 141, 61
- Galleti, S., Bellazzini, M., Buzzoni, A., Federici, L., & Fusi Pecci, F. 2009, *A&A*, 508, 1285
- Galleti, S., Bellazzini, M., Federici, L., Buzzoni, A., & Fusi Pecci, F. 2007, *A&A*, 471, 127
- Galleti, S., Federici, L., Bellazzini, M., Buzzoni, A., & Fusi Pecci, F. 2006, *A&A*, 456, 985
- Galleti, S., Federici, L., Bellazzini, M., Fusi Pecci, F., & Macrina, S. 2004, *A&A*, 416, 917
- Georgakakis, A., Nandra, K., Laird, E. S., Aird, J., & Trichas, M. 2008, *MNRAS*, 388, 1205
- Gladstone, J., Done, C., Gierliński, M. 2007, *MNRAS*, 378, 13
- Grimm, H.-J., Gilfanov, M., & Sunyaev, R. 2003, *MNRAS*, 339, 793
- Kaur, A., Henze, M., Pietsch, W., et al. 2012, *A&A*, 538, 6
- Lin, D., Remillard, R. A., & Homan, J. 2007, *ApJ*, 667, 1073
- Lin, D., Remillard, R. A., & Homan, J. 2009, *ApJ*, 696, 1257
- Lin, D., Remillard, R. A., Homan, J., & Barret, D. 2012, *ApJ*, 756, 34
- Markowitz, A. & Edelson, R. 2004, *ApJ*, 617, 939
- Marshall, N., Warwick, R. S., & Pounds, K. A. 1981, *MNRAS*, 194, 987
- Massey, P., Olsen, K. A. G., Hodge, P. W., et al. 2006, *AJ*, 131, 2478
- Middleton, M. J., Miller-Jones, J. C. A., Markoff, S., et al. 2013, *Nature*, 493, 187
- Munro, M. P., Remillard, R. A., & Chakrabarty, D. 2002, *ApJ*, 568, L35
- Nandra, K., George, I. M., Mushotzky, R. F., Turner, T. J., & Yaqoob, T. 1997, *ApJ*, 476, 70
- Noorae, N., Callanan, P. J., Barnard, R., et al. 2012, *A&A*, 542, A120
- Puccetti, S., Capalbi, M., Giommi, P., et al. 2011, *A&A*, 528, A122
- Remillard, R. A. & McClintock, J. E. 2006, *ARA&A*, 44, 49
- Stanek, K. Z. & Garnavich, P. M. 1998, *ApJ*, 503, L131
- Stark, A. A., Gammie, C. F., Wilson, R. W. et al. 1992, *ApJS*, 79, 77
- Stiele, H., Pietsch, W., Haberl, F., Freyberg, M. 2008, *A&A*, 480, 599
- Stiele, H., Pietsch, W., Haberl, F., et al. 2011, *A&A*, 534, A55
- Tananbaum, H., Peters, G., Forman, W., et al. 1978, *ApJ*, 223, 74
- Tang, J., Yu, W.-F., Yan, Z., 2011, *RAA*, 11, 434
- Vagnetti, F., Turriziani, S., & Trevese, D. 2011, *A&A*, 536, A84
- van der Klis, M. 1994, *ApJS*, 92, 511
- Voss, R. & Gilfanov, M. 2007, *MNRAS*, 380, 1685
- Wang, Q. D. 2004, *ApJ*, 612, 159
- Watson, M. G., Schröder, A. C., Fyfe, D., et al. 2009, *A&A*, 493, 339

Table 1
continued.

Src	Pos	σ_{RA}''	σ_{Dec}''	O_A	O_H	Properties	$L_{con}/10^{37}$	χ^2/dof	SF Rank
61	00:41:59.30 +41:05:39.0			15	0	NE=X	0.09±0.02	7/14	0.0 ^g
62	00:41:59.43 +41:20:46.9 ^a	1.5 ^a	1.5 ^a	39	39	H	0.072±0.009 ^d	50/77	0.0 ^g
63	00:42:00.58 +41:14:08.7	0.6	0.8	52	27	NE	0.041±0.006	63/78	0.0 ^g
64	00:42:00.78 +41:16:31.9	0.7	0.8	52	33	NE	0.038±0.006	45/84	0.0 ^g
65	00:42:02.83 +41:27:57.6 ^a	1.8 ^a	1.8 ^a	6	31	NC	0.066±0.014	26/36	0.6 ^g
66	00:42:02.93 +41:23:15.5 ^a	1.9 ^a	1.9 ^a	25	37	H	0.109±0.012 ^d	60/61	3.3 ^f
67	00:42:04.12 +41:09:29.4	0.6	0.6	32	53	NE	0.131±0.012 ^d	90/84	0.1 ^g
68	00:42:04.16 +41:15:32.1	0.3	0.3	88	49	H	0.145±0.008	122/136	0.0 ^g
69	00:42:04.30 +41:09:04.31	1.0	0.6	21	38	NE	0.129±0.014 ^d	43/58	3.4 ^f
70	00:42:04.77 +41:29:33.70 ^a	1.7 ^a	1.7 ^a	6	28	H	0.043±0.014	21/33	0.0 ^g
71	00:42:05.77 +41:13:30.43	0.3	0.4	59	41	T	0.084±0.008	1069/99	88.4 ^f
72	00:42:05.84 +41:11:34.25	0.5	0.4	58	37	H	0.085±0.008 ^d	81/94	0.0 ^g
73	00:42:06.07 +41:02:47.38	0.7	0.9	18	48	Gal	0.080±0.010 ^d	87/65	2.6 ^g
74	00:42:07.09 +41:17:20.25	0.4	0.3	86	51	H=[*],*	0.083±0.005 ^{c e}	87/85	0.0
75	00:42:07.1 +41:00:17 ^a	3 ^a	3 ^a	14	13	Gal	0.046±0.010 ^d	62/26	12.3 ^g
76	00:42:07.32 +41:00:55.0	1.0	0.8	15	14	NE=X	0.12±0.03	20/28	0.0 ^g
77	00:42:07.64 +41:10:27.5	0.5	0.5	68	51	H	0.188±0.010	120/118	0.6 ^g
78	00:42:07.786 +41:18:15.07	0.12	0.10	96	62	H	5.13±0.03	850/157	4.3 ^f
79	00:42:07.89 +41:04:36.7	0.9	0.6	24	56	H	0.80±0.03 ^d	98/79	5.2 ^f
80	00:42:08.20 +41:12:50.1	0.5	0.3	76	33	H	0.066±0.006 ^d	88/108	0.0 ^g
81	00:42:08.41 +41:03:38.4	0.8	0.9	15	39	NE	0.15±0.03 ^d	49/53	0.0 ^g
82	00:42:08.98 +41:23:30.0	0.8	0.7	22	28	*	0.054±0.008 ^d	52/49	1.1
83	00:42:09.12 +41:20:48.3	0.2	0.2	89	61	H	1.16±0.02 ^d	820/149	292.0 ^f
84	00:42:09.530 +41:17:45.55	0.14	0.10	96	61	GC, XB	1.65±0.03	1191/156	258.0 ^f
85	00:42:09.63 +41:20:08.8	0.5	0.5	77	39	NE=[SNR]	0.049±0.005	99/115	0.3
86	00:42:10.19 +41:21:26.1	0.5	0.7	58	26	NE	0.044±0.006	53/83	0.0 ^g
87	00:42:10.314 +41:15:09.9	0.19	0.2	93	58	H=[*],H	0.335±0.008	653/150	>320 ^f
88	00:42:10.77 +41:06:47.8	0.5	0.5	21	40	[XB]	0.089±0.013 ^d	66/60	7.6 ^f
89	00:42:10.96 +41:12:48.0	0.2	0.2	91	60	H	0.220±0.008	168/150	5.0 ^f
90	00:42:11.37 +41:04:25.5	0.5	0.4	19	53	NE=T	0.65±0.03	2292/71	16.2 ^f
91	00:42:11.450 +41:30:24.80 ^a	1.5 ^a	1.5 ^a	3	52	H	0.187±0.014	988/54	3.7 ^f
92	00:42:11.754 +41:10:49.0	0.2	0.2	65	0	H=[*],H	0.580±0.017	287/64	7.7 ^f
93	00:42:11.973 +41:16:48.78	0.19	0.10	96	57	H	0.349±0.009	229/152	9.7 ^f
94	00:42:12.08 +41:29:50.4 ^a	1.2 ^a	1.2 ^a	4	35	[SSS]	0.043±0.010	59/38	1.3
95	00:42:12.186 +41:17:58.71	0.1	0.10	97	62	[GC]=GC, XB	1.41±0.02	3517/158	>320 ^f
96	00:42:12.34 +41:29:30.1 ^a	1.3 ^a	1.3 ^a	5	34	[Gal]	0.046±0.010	37/38	0.0 ^g
97	00:42:12.74 +41:12:44.3	0.5	0.3	81	47	NE=X	0.058±0.005	99/127	0.0 ^g
98	00:42:12.74 +41:05:57.3 ^a	1.2 ^a	1.2 ^a	21	34	[*]=*	0.065±0.011	50/54	2.1
99	00:42:13.02 +41:16:28.2	0.3	0.2	85	39	NE=X	0.052±0.004	90/123	0.4 ^g
100	00:42:13.169 +41:18:36.52	0.1	0.10	97	62	H	3.49±0.02	4784/158	259.0 ^f
101	00:42:14.73 +41:22:13.2	0.7	0.7	55	40	NE	0.040±0.005	56/94	0.0 ^g
102	00:42:15.00 +41:21:21.3	0.5	0.5	81	34	NE=[GC]	0.062±0.005	83/114	>320 ^f
103	00:42:15.154 +41:12:34.51	0.1	0.10	92	62	H	1.33±0.02	4762/153	>320 ^f
104	00:42:15.266 +41:18:01.2	0.2	0.2	95	57	H	0.188±0.007 ^d	193/151	10.7 ^f
105	00:42:15.50 +40:57:29.4	0.8	0.8	4	3	NE	0.169±0.078	4/6	3.4 ^f
106	00:42:15.526 +41:20:31.6	0.17	0.2	100	62	[GC]	0.469±0.010	269/161	2.3 ^f
107	00:42:15.57 +41:31:13.1 ^a	0.8 ^a	0.8 ^a	5	29	H	0.083±0.013	24/33	0.0 ^g
108	00:42:15.704 +41:17:20.93	0.12	0.10	95	47	H	1.081±0.019	1949/141	>320 ^f
109	00:42:15.79 +41:01:14.2	0.3	0.4	19	58	GC=BHC	21.0±0.2	230/76	14.5 ^f
110	00:42:16.08 +41:15:53.3	0.4	0.3	46	31	NE	0.020±0.003	76/76	1.4 ^g
111	00:42:16.10 +41:19:26.4	0.16	0.3	46	34	NE=X, T	0.040±0.005 ^d	234/79	27.3 ^f
112	00:42:16.13 +41:22:13.9	0.9	0.7	65	32	NE=X	0.037±0.005 ^d	59/96	0.0 ^g
113	00:42:16.45 +41:14:30.6	0.5	0.5	67	38	NE	0.040±0.004	59/104	0.0 ^g
114	00:42:16.54 +41:16:10.8	0.6	0.5	69	31	NE=X	0.033±0.004	64/99	0.0 ^g
115	00:42:17.01 +41:18:56.6	0.5	0.4	76	39	NE=X	0.029±0.004	49/114	0.0 ^g
116	00:42:17.050 +41:15:08.29	0.17	0.10	53	43	NE=T	0.053±0.006	1608/95	3.2 ^f
117	00:42:17.311 +41:15:37.33	0.14	0.10	58	42	NE=T	0.027±0.004	3957/99	0.6 ^f
118	00:42:18.07 +41:08:59.5	0.8	0.6	50	37	NE	0.037±0.005	54/86	1.7 ^g
119	00:42:18.33 +41:02:10.3	1.0	1.0	14	36	NE	0.14±0.03 ^d	24/49	0.0 ^g
120	00:42:18.355 +41:12:23.68	0.1	0.10	93	62	H	7.29±0.05	3140/154	164.0 ^f
121	00:42:18.41 +40:58:51.7	0.7	0.7	7	20	NE	0.13±0.03 ^c	2/6	0.0 ^g
122	00:42:18.648 +41:14:01.85	0.11	0.10	92	63	GC=BHC	5.51±0.04	1527/154	2.2 ^f
123	00:42:18.82 +41:29:27.3 ^a	0.8 ^a	0.8 ^a	6	46	[AGN]	0.222±0.014	67/51	>320 ^f
124	00:42:18.83 +41:26:47.2 ^a	1.2 ^a	1.2 ^a	9	43	[SSS]=[*]	0.043±0.009	37/51	>320
125	00:42:19.02 +41:20:04.5	0.4	0.4	91	37	H	0.038±0.004 ^d	106/127	2.9 ^f
126	00:42:19.46 +41:08:03.0	0.9	0.8	38	38	NE=X	0.065±0.008 ^d	45/75	0.8 ^g
127	00:42:19.59 +41:13:34.3	0.5	0.4	80	35	NE	0.049±0.005	68/114	0.0 ^g
128	00:42:19.77 +41:21:54.1	0.4	0.4	84	32	GC	0.055±0.004 ^d	142/115	23.2 ^f
129	00:42:20.10 +41:08:24.2	0.6	0.6	44	41	NE=X	0.049±0.008 ^d	50/84	0.0 ^g
130	00:42:20.28 +41:07:14.1 ^a	1.5 ^a	1.5 ^a	28	30	NC	0.044±0.007	51/57	0.0 ^g

Table 1
continued.

Src	Pos	σ_{RA}'''	σ_{Dec}'''	O_A	O_H	Properties	$L_{con} / 10^{37}$	χ^2/dof	SF Rank
131	00:42:20.43 +41:13:13.7	0.5	0.4	69	38	NE=X	0.041±0.006	66/106	0.0 ^g
132	00:42:20.56 +41:26:39.3	0.5	0.5	14	58	NE=X	0.366±0.013	76/71	6.4 ^f
133	00:42:20.63 +40:57:13.4	0.9	0.7	4	7	NE	0.16±0.05 ^c	4/3	0.6 ^g
134	00:42:20.68 +41:16:07.8	0.4	0.4	59	28	NE=T	0.021±0.003	83/86	3.1 ^f
135	00:42:20.80 +41:13:44.1	0.4	0.3	69	34	NE	0.036±0.005	56/102	0.0 ^g
136	00:42:20.82 +41:17:57.3	0.6	0.6	39	41	NE	0.020±0.003	69/79	1.7 ^g
137	00:42:20.90 +41:15:20.1	0.5	0.4	40	0	NE=T	0.055±0.010	140/39	4.1 ^f
138	00:42:20.95 +41:22:55.1 ^a	1.9 ^a	1.9 ^a	62	34	H=[*],[*]	0.030±0.005	53/95	0.5
139	00:42:21.24 +41:07:18.1	0.3	0.3	33	36	NE	0.049±0.008	69/68	0.0 ^g
140	00:42:21.312 +41:15:52.46	0.2	0.10	71	35	NE	0.033±0.003	1472/105	6.5 ^f
141	00:42:21.3 +41:24:11 ^a	2 ^a	2 ^a	35	29	H	0.023±0.006	45/63	0.0 ^g
142	00:42:21.492 +41:16:01.29	0.11	0.10	103	62	H	5.59±0.04	2288/164	94.0 ^f
143	00:42:21.568 +41:14:19.72	0.14	0.10	99	57	NE=[GC],T	0.254±0.008	935/155	>320 ^f
144	00:42:21.63 +41:12:17.2 ^a	1.5 ^a	1.5 ^a	52	37	[SSS]=[Nova]	0.034±0.007	58/88	0.0
145	00:42:21.80 +41:15:02.3	0.3	0.2	83	33	NE	0.039±0.004	80/115	2.0 ^g
146	00:42:22.32 +40:59:25.4	0.7	0.7	15	26	H	3.28±0.10	135/40	6.1 ^f
147	00:42:22.34 +41:13:45.2	0.3	0.3	40	30	NE=Nova,T	0.019±0.003 ^d	232/69	0.0
148	00:42:22.424 +41:13:34.03	0.12	0.10	98	61	H	1.906±0.019	1684/158	132.6 ^f
149	00:42:22.44 +40:57:43.6	0.7	0.9	10	8	NE=T	0.33±0.03 ^d	118/17	7.7 ^f
150	00:42:22.73 +41:22:34.3	0.5	0.5	62	27	NE=X	0.031±0.005 ^d	59/88	0.0 ^g
151	00:42:22.954 +41:15:35.23	0.11	0.10	105	62	XB,BHC	9.40±0.04	28720/166	>320 ^f
152	00:42:23.02 +41:07:38.7	0.5	0.5	56	57	H	0.226±0.011	168/112	0.0 ^g
153	00:42:23.149 +41:14:07.53	0.12	0.10	101	62	H	1.087±0.013	1760/162	>320 ^f
154	00:42:24.41 +41:17:29.8 ^a	0.9 ^a	0.9 ^a	83	52	!SNR	0.068±0.006	120/134	0.0 ^g
155	00:42:24.57 +41:24:01.9	0.3	0.4	61	53	[XB]	0.081±0.006	841/113	187.7 ^f
156	00:42:24.978 +41:18:16.43	0.6	0.6	31	36	NE	0.011±0.002	52/66	1.9 ^g
157	00:42:25.1 +40:57:18 ^a	3 ^a	3 ^a	6	8	GC	0.08±0.02	34/13	0.8 ^f
158	00:42:25.136 +41:13:40.58	0.12	0.10	103	60	[*]=var*	0.770±0.013	1764/162	>320
159	00:42:26.070 +41:19:15.03	0.12	0.10	106	62	GC=BHC	2.033±0.018	3999/167	>320 ^f
160	00:42:26.24 +41:25:52.0	0.3	0.3	35	60	H	1.28±0.03	293/94	15.0 ^f
161	00:42:26.48 +41:13:46.6	0.5	0.4	49	23	NE=X	0.013±0.003 ^d	58/71	0.0 ^g
162	00:42:26.50 +41:23:52.0	0.6	0.6	54	35	NE	0.042±0.005 ^d	58/88	0.1 ^g
163	00:42:27.38 +40:59:35.9	1.0	0.9	10	30	GC	0.038±0.011	31/39	1.8 ^f
164	00:42:27.46 +41:14:52.8	0.3	0.2	51	36	NE	0.022±0.003	138/86	0.5 ^g
165	00:42:27.67 +41:20:48.1	0.2	0.4	87	43	H=[*],[*]	0.055±0.003	88/129	5.9
166	00:42:27.94 +41:18:17.8	0.4	0.3	69	34	NE	0.020±0.003	64/102	1.0 ^g
167	00:42:28.193 +41:10:00.30	0.12	0.10	96	62	[XB]=BHC	3.85±0.03	568/157	0.0 ^f
168	00:42:28.285 +41:12:22.95	0.11	0.10	101	62	H=BHC	4.55±0.03	5639/162	6.0 ^f
169	00:42:28.33 +41:14:49.1	0.3	0.3	55	23	NE=X,T	0.020±0.004	1013/77	3.3 ^f
170	00:42:28.88 +41:17:41.2	0.4	0.5	41	28	NE	0.014±0.002	45/68	0.0 ^g
171	00:42:28.91 +41:04:35.8	0.5	0.6	24	62	H	3.07±0.04	1293/85	59.0 ^f
172	00:42:29.10 +41:13:48.5	0.3	0.4	52	42	NE	0.039±0.004	302/93	49.1 ^f
173	00:42:29.12 +41:15:47.2	0.3	0.2	72	34	NE	0.036±0.005 ^d	118/105	0.0 ^g
174	00:42:29.25 +41:26:40.4 ^a	1.0 ^a	1.0 ^a	15	46	[*]=*	0.045±0.008	52/60	1.0
175	00:42:29.46 +41:29:02.4 ^a	0.7 ^a	0.7 ^a	8	58	*	0.55±0.03	170/65	52.6
176	00:42:29.82 +41:17:57.5	0.5	0.6	25	27	NE=GC	0.010±0.003 ^d	46/51	19.8 ^f
177	00:42:30.279 +41:16:53.3	0.2	0.2	96	43	NE=var*	0.069±0.003	114/138	2.5
178	00:42:30.976 +41:19:10.51	0.16	0.10	105	52	H	0.079±0.003	130/156	2.1 ^g
179	00:42:31.147 +41:16:21.67	0.11	0.10	107	62	H=BHC	7.87±0.04	669/168	0.5 ^f
180	00:42:31.19 +41:04:36.1	0.6	0.6	24	55	H	0.232±0.013	95/78	1.6 ^g
181	00:42:31.271 +41:19:38.99	0.11	0.10	108	62	GC	2.38±0.02	3988/169	>320 ^f
182	00:42:31.339 +41:20:08.0	0.2	0.2	99	46	![GC]	0.057±0.003	125/144	0.6 ^g
183	00:42:32.07 +41:23:05.7	0.6	0.5	84	43	H	0.045±0.005	126/126	0.0 ^g
184	00:42:32.072 +41:13:14.33	0.11	0.10	106	62	NE=X	5.48±0.05 ^c	2095/10581.0 ^f	
185	00:42:32.11 +41:19:13.4	0.3	0.2	76	40	NE	0.029±0.003	58/115	0.0 ^g
186	00:42:32.536 +41:15:45.54	0.16	0.10	19	40	NE=var*	0.038±0.006	42/58	0.0
187	00:42:32.61 +41:14:31.1	0.4	0.4	59	39	NE	0.020±0.004	51/97	3.5 ^f
188	00:42:32.747 +41:13:10.79	0.12	0.10	106	60	H	0.726±0.011	587/165	185.1 ^f
189	00:42:33.11 +41:03:28.1	0.7	0.7	22	52	GC	0.123±0.010 ^d	103/73	14.6 ^f
190	00:42:33.23 +41:06:48.4	0.7	0.9	33	37	H	0.068±0.009	59/69	6.7 ^f
191	00:42:33.419 +41:17:03.51	0.14	0.10	52	34	NE=XB,T	0.014±0.003 ^d	311/85	0.0 ^f
192	00:42:33.55 +41:21:38.7	0.4	0.4	85	54	*	0.064±0.004 ^d	218/138	5.3
193	00:42:33.90 +41:23:31.7	0.2	0.2	67	38	[XB]=T	0.055±0.005	2082/104	181.0 ^f
194	00:42:33.90 +41:20:40.6	0.4	0.6	67	34	NE	0.024±0.003	56/100	0.0 ^g
195	00:42:33.898 +41:16:19.82	0.11	0.10	107	62	H	1.099±0.013 ^d	518/168	8.7 ^f
196	00:42:34.19 +41:21:49.8	0.2	0.2	105	55	H	0.265±0.007	228/159	6.7 ^f
197	00:42:34.45 +41:18:09.9	0.2	0.2	29	41	BHC,T	0.013±0.002	168/69	16.8 ^f
198	00:42:34.63 +41:32:52.4 ^a	0.6 ^a	0.6 ^a	7	31	GC	1.54±0.06	134/37	14.7 ^f
199	00:42:34.67 +40:57:08.9	0.8	0.9	13	14	GC=BHC,T	0.44±0.05 ^d	664/26	11.9 ^f
200	00:42:34.767 +41:15:23.19	0.14	0.10	63	39	NE=var*	0.028±0.004	231/101	11.3

Table 1
continued.

Src	Pos	σ_{RA}''	σ_{Dec}''	O_A	O_H	Properties	$L_{con}/10^{37}$	χ^2/dof	SF Rank
201	00:42:35.232 +41:20:05.86	0.11	0.10	108	61	H	1.707 \pm 0.019	907/168	33.8 ^f
202	00:42:35.88 +41:10:07.9	0.6	0.6	74	38	H	0.038 \pm 0.005 ^d	74/111	0.0 ^g
203	00:42:36.06 +41:20:21.8	0.6	0.5	56	41	NE	0.025 \pm 0.004	72/96	0.0 ^g
204	00:42:36.33 +40:58:48.0	0.8	0.8	11	14	H	0.28 \pm 0.05	28/24	4.4 ^f
205	00:42:36.611 +41:13:50.24	0.14	0.10	98	56	[*]=var*	0.095 \pm 0.004 ^e	581/153	7.9
206	00:42:37.05 +41:14:28.2	0.4	0.3	52	41	NE=[Nova]	0.021 \pm 0.003	1063/92	175.4
207	00:42:37.88 +41:21:33.9	0.5	0.5	72	31	NE	0.040 \pm 0.004	77/102	1.3 ^g
208	00:42:38.05 +41:05:25.2	0.6	0.7	25	45	H	0.242 \pm 0.016 ^d	65/69	1.6 ^g
209	00:42:38.594 +41:16:03.71	0.11	0.10	107	62	XB	32.78 \pm 0.16 ^c	1255/106	0.0 ^f
210	00:42:38.68 +41:17:23.9	0.2	0.2	63	35	NE	0.027 \pm 0.003 ^d	128/97	3.1 ^f
211	00:42:38.75 +41:15:26.5	0.3	0.2	76	37	NE=X	0.035 \pm 0.004	64/112	0.0 ^g
212	00:42:39.24 +41:14:24.7	0.2	0.2	80	42	H	0.039 \pm 0.002	78/121	0.0 ^g
213	00:42:39.536 +41:14:28.47	0.11	0.10	106	61	H	0.797 \pm 0.011	2089/166	>320 ^f
214	00:42:39.585 +41:16:14.30	0.11	0.10	65	30	NE=X,BHC,T	0.051 \pm 0.005	3482/94	58.0 ^f
215	00:42:39.66 +41:17:00.9	0.2	0.2	77	42	NE=X	0.035 \pm 0.003	85/118	6.2 ^f
216	00:42:39.76 +41:14:54.1	0.6	0.5	53	33	NE	0.030 \pm 0.005	75/85	0.0 ^g
217	00:42:39.995 +41:15:47.54	0.11	0.10	107	62	H	2.17 \pm 0.02 ^c	2270/106	>320 ^f
218	00:42:40.02 +41:28:36.7 ^a	1.3 ^a	1.3 ^a	12	38	H	0.051 \pm 0.008	42/49	5.9 ^f
219	00:42:40.229 +41:18:45.26	0.11	0.10	109	62	H	1.633 \pm 0.017	2289/170	>320 ^f
220	00:42:40.46 +41:15:46.1	0.3	0.3	58	29	H=T	0.017 \pm 0.003	213/86	0.1 ^f
221	00:42:40.51 +41:13:55.3	0.4	0.3	50	35	NE=X	0.017 \pm 0.003	70/84	0.0 ^g
222	00:42:40.64 +41:10:33.4	0.2	0.2	101	58	GC	0.095 \pm 0.004	442/158	>320 ^f
223	00:42:40.654 +41:13:27.32	0.11	0.10	107	61	H=BHC	1.332 \pm 0.014	4983/167	>320 ^f
224	00:42:40.75 +41:10:05.1	0.5	0.5	61	41	NE=*	0.025 \pm 0.003	100/101	5.0
225	00:42:40.95 +41:22:16.6	0.4	0.4	73	39	[*]=*	0.019 \pm 0.003	56/111	0.0
226	00:42:41.07 +41:11:02.0	0.4	0.4	77	39	NE=X	0.035 \pm 0.004	61/115	2.0 ^g
227	00:42:41.08 +41:07:01.8	0.4	0.7	50	44	H	0.070 \pm 0.007	72/93	0.0 ^g
228	00:42:41.161 +41:18:21.44	0.14	0.10	31	33	NE=T	0.011 \pm 0.002	201/63	14.6 ^f
229	00:42:41.442 +41:15:23.82	0.12	0.10	106	60	GC	0.358 \pm 0.009	719/165	195.3 ^f
230	00:42:41.480 +41:16:17.85	0.12	0.10	76	40	NE	0.001 \pm 0.004	1/115	0.0 ^g
231	00:42:41.622 +41:14:36.89	0.12	0.10	59	35	NE=T	0.037 \pm 0.004	981/93	166.3 ^f
232	00:42:41.674 +41:21:05.48	0.14	0.10	108	60	H	0.367 \pm 0.007	447/167	62.0 ^f
233	00:42:41.800 +41:16:35.88	0.12	0.10	65	36	BHC,T	0.029 \pm 0.004	317/100	2.0 ^f
234	00:42:41.96 +41:28:34.8 ^a	1.1 ^a	1.1 ^a	14	42	H	0.070 \pm 0.008	46/55	1.4 ^g
235	00:42:42.082 +41:15:32.03	0.12	0.10	107	61	NE=X	0.254 \pm 0.006	836/167	28.4 ^f
236	00:42:42.177 +41:16:08.23	0.11	0.10	56	40	BHC,T	0.036 \pm 0.005	2319/95	102.0 ^f
237	00:42:42.24 +41:19:14.1	0.2	0.2	72	37	NE=X	0.021 \pm 0.002	62/108	0.0 ^g
238	00:42:42.329 +41:14:45.43	0.11	0.10	108	62	H	1.373 \pm 0.013	601/169	6.7 ^f
239	00:42:42.365 +41:15:45.02	0.2	0.2	69	43	NE=X	0.030 \pm 0.004	157/111	1.3 ^g
240	00:42:42.430 +41:12:19.20 ^a	1.4 ^a	1.4 ^a	70	33	[SSS]=var*	0.025 \pm 0.005	53/102	0.0
241	00:42:42.481 +41:15:53.67	0.11	0.10	109	62	NE	2.36 \pm 0.03 ^c	136/108	0.0 ^g
242	00:42:42.534 +41:16:59.42	0.12	0.10	106	59	NE=[SNR]	0.214 \pm 0.005	542/164	48.5 ^f
243	00:42:42.65 +41:14:05.0	0.3	0.2	71	42	NE	0.026 \pm 0.003	71/112	0.0 ^g
244	00:42:42.65 +41:16:45.7	0.3	0.3	70	27	NE	0.025 \pm 0.003	68/96	0.4 ^g
245	00:42:42.72 +41:14:55.4	0.2	0.3	46	25	NE=X,T	0.020 \pm 0.003	721/70	13.3 ^f
246	00:42:42.81 +41:19:40.0	0.6	0.6	35	31	NE=X	0.009 \pm 0.002	48/65	0.3 ^g
247	00:42:43.001 +41:15:43.14	0.11	0.10	109	62	H	1.68 \pm 0.02 ^c	160/108	0.0 ^g
248	00:42:43.126 +41:16:04.07	0.14	0.10	71	42	NE	0.037 \pm 0.004	162/112	1.5 ^g
249	00:42:43.202 +41:16:40.26	0.12	0.10	74	45	NE=[SNR],T	0.094 \pm 0.008	856/118	230.0 ^f
250	00:42:43.300 +41:13:19.43	0.12	0.10	94	46	NC=[SNR]	0.055 \pm 0.003	869/139	269.0 ^f
251	00:42:43.683 +41:25:18.53	0.20	0.10	41	29	NE=T,U	0.396 \pm 0.016	61651/69	8.0 ^f
252	00:42:43.753 +41:16:32.41	0.11	0.10	109	62	[XB]	2.088 \pm 0.016	2825/170	62.6 ^f
253	00:42:43.791 +41:15:14.15	0.12	0.10	48	35	NE	0.120 \pm 0.005	1003/82	140.3 ^f
254	00:42:43.870 +41:16:03.84	0.11	0.10	109	62	NE=X	0.708 \pm 0.010	1022/170	81.0 ^f
255	00:42:43.879 +41:16:29.62	0.12	0.10	109	62	[XB]	0.736 \pm 0.010	2499/170	>320 ^f
256	00:42:43.930 +41:16:10.75	0.12	0.10	67	47	NE=X,T	0.102 \pm 0.004	3291/113	2.2 ^f
257	00:42:43.971 +41:17:55.60	0.13	0.10	37	29	[SSS]=Nova	0.023 \pm 0.004	59/65	0.0
258	00:42:44.114 +41:16:04.14	0.11	0.10	55	36	NE=T	0.023 \pm 0.003	159/90	4.2 ^f
259	00:42:44.297 +41:16:14.00	0.12	0.10	109	62	NE	0.187 \pm 0.004	188/170	2.9 ^f
260	00:42:44.379 +41:11:58.28	0.12	0.10	106	59	H	0.367 \pm 0.007	1075/164	>320 ^f
261	00:42:44.42 +40:59:58.3	0.5	0.8	11	17	H	0.18 \pm 0.04 ^d	28/27	6.8 ^f
262	00:42:44.43 +41:28:11.2 ^a	0.6 ^a	0.6 ^a	13	36	[XB]	0.054 \pm 0.008	230/48	4.6 ^f
263	00:42:44.62 +41:18:03.1	0.4	0.3	50	33	NE=X	0.016 \pm 0.002	50/82	0.1 ^g
264	00:42:44.677 +41:16:18.12	0.11	0.10	109	61	NE=X	0.529 \pm 0.008	397/169	10.5 ^f
265	00:42:44.831 +41:11:37.89	0.11	0.10	106	62	H=XB,BHC	3.62 \pm 0.02	3701/167	244.1 ^f
266	00:42:44.905 +41:17:39.76	0.11	0.10	109	59	H	0.578 \pm 0.009	297/167	0.0 ^g
267	00:42:45.091 +41:14:07.10	0.12	0.10	96	58	[XB]	0.064 \pm 0.003	1570/153	7.8 ^f
268	00:42:45.093 +41:15:23.10	0.12	0.10	106	60	NE	0.252 \pm 0.006 ^d	444/165	8.3 ^f
269	00:42:45.122 +41:16:21.68	0.11	0.10	109	62	NE=BHC	2.158 \pm 0.017	3625/170	>320 ^f
270	00:42:45.22 +41:15:41.9	0.5	0.3	75	38	NE	0.145 \pm 0.007	716/112	202.0 ^f

Table 1
continued.

Src	Pos	σ_{RA}''	σ_{Dec}''	O_A	O_H	Properties	$L_{con}/10^{37}$	χ^2/dof	SF Rank
271	00:42:45.230 +41:17:22.38	0.11	0.10	96	52	T	0.190±0.005	4052/147	>320 ^f
272	00:42:45.237 +41:16:11.12	0.11	0.10	109	62	NE=X	0.266±0.005	679/170	27.6 ^f
273	00:42:45.526 +41:16:52.60	0.4	0.3	66	39	NE	0.026±0.004	53/104	0.5 ^g
274	00:42:45.598 +41:16:08.59	0.11	0.10	109	61	NE=X	0.518±0.009	1594/169	>320 ^f
275	00:42:45.84 +41:24:33.4	0.5	0.5	74	35	H	0.111±0.008	67/108	1.2 ^g
276	00:42:45.946 +41:10:36.53	0.12	0.10	56	43	NE=BHC,T	0.069±0.006	8381/98	118.4 ^f
277	00:42:46.007 +41:16:19.59	0.11	0.10	97	49	NE=X,T	0.138±0.004	1981/145	4.3 ^f
278	00:42:46.100 +41:17:36.33	0.12	0.10	86	46	NE=GC,T	0.072±0.004 ^d	546/131	>320 ^f
279	00:42:46.11 +41:17:28.7	0.4	0.4	61	37	NE	0.022±0.003	57/97	0.0 ^g
280	00:42:46.160 +41:15:43.15	0.12	0.10	108	60	NE	0.302±0.007	285/167	15.0 ^f
281	00:42:46.33 +41:28:23.6 ^a	1.8 ^a	1.8 ^a	13	32	H	0.047±0.009	27/44	6.6 ^f
282	00:42:46.36 +41:27:23.6 ^a	1.9 ^a	1.9 ^a	21	27	H=[*],[*]	0.042±0.007 ^d	44/47	5.5
283	00:42:46.433 +41:16:10.07	0.13	0.10	62	41	NE=T	0.029±0.003	1918/102	0.0 ^f
284	00:42:46.76 +41:07:33.5	1.3	0.9	34	32	NE	0.032±0.006	44/65	0.6 ^g
285	00:42:46.93 +41:21:19.4	0.2	0.2	106	52	H	0.155±0.005 ^d	318/157	212.5 ^f
286	00:42:46.969 +41:16:15.58	0.11	0.10	109	62	!AGN=BHC	3.17±0.02	3472/170	106.0 ^f
287	00:42:47.16 +41:14:07.0	0.2	0.2	71	43	NE=T	0.073±0.006	2289/113	3.9 ^f
288	00:42:47.17 +41:14:13.0	0.3	0.3	54	39	[SSS]	0.024±0.003	82/92	1.4
289	00:42:47.176 +41:16:28.41	0.11	0.10	103	62	[XB]=BHC	7.32±0.04	16817/164	>320 ^f
290	00:42:47.240 +41:11:57.70	0.17	0.10	105	55	NE=X	0.134±0.005 ^d	386/159	51.8 ^f
291	00:42:47.441 +41:15:07.52	0.18	0.10	60	36	NE=Nova	0.021±0.003	92/95	1.2
292	00:42:47.55 +40:58:37.5	0.8	0.6	7	14	NE	0.20±0.05	24/20	7.4 ^f
293	00:42:47.795 +41:11:13.67	0.17	0.10	51	37	[GC]=GC,T	0.020±0.003	2348/87	86.5 ^f
294	00:42:47.869 +41:16:22.99	0.12	0.10	103	56	NE	0.121±0.004	448/158	10.8 ^f
295	00:42:47.89 +41:10:52.6	0.3	0.3	91	45	NE=X	0.061±0.003	123/135	2.1 ^g
296	00:42:47.886 +41:15:49.72	0.11	0.10	88	56	T	0.091±0.004	3607/143	>320 ^f
297	00:42:47.893 +41:15:32.87	0.11	0.10	109	62	H=BHC	2.664±0.019	4602/170	>320 ^f
298	00:42:48.31 +41:20:33.1	0.5	0.4	70	34	NE	0.020±0.003 ^d	65/103	3.7 ^f
299	00:42:48.529 +41:15:21.12	0.11	0.10	109	62	H=BHC	9.92±0.04	842/170	9.3 ^f
300	00:42:48.546 +41:25:22.1	0.2	0.2	69	59	T=BHC	1.48±0.02	9096/127	>320 ^f
301	00:42:48.720 +41:16:24.44	0.12	0.10	108	58	NE=X	0.246±0.005	578/165	205.8 ^f
302	00:42:48.90 +41:17:45.9	0.4	0.4	42	30	NE=X	0.012±0.002	39/71	0.3 ^g
303	00:42:49.03 +41:19:46.4	0.4	0.4	80	39	NE=X	0.037±0.003	62/118	0.0 ^g
304	00:42:49.05 +41:24:07.4	0.5	0.5	84	57	SNR	0.084±0.006	173/140	1.0
305	00:42:49.155 +41:17:42.05	0.12	0.10	85	47	NE=X	0.041±0.003	1484/131	267.0 ^f
306	00:42:49.236 +41:16:01.16	0.12	0.10	89	49	NE=T	0.190±0.006	5386/137	>320 ^f
307	00:42:49.245 +41:18:16.00	0.11	0.10	109	62	H	1.140±0.013	1465/170	103.0 ^f
308	00:42:49.32 +41:08:26.4	0.7	0.6	66	37	NE	0.037±0.005	57/102	0.0 ^g
309	00:42:49.45 +41:22:34.9	0.5	0.5	76	35	H	0.046±0.005	75/110	0.9 ^g
310	00:42:49.51 +41:06:34.1	0.8	0.8	33	36	H	0.102±0.010	50/68	1.3 ^g
311	00:42:49.76 +41:16:33.1 ^a	0.8 ^a	0.8 ^a	54	32	[SSS]=[Nova]	0.042±0.006 ^e	461/85	0.0
312	00:42:49.97 +41:11:08.8	0.3	0.3	84	37	H	0.031±0.003 ^d	136/120	45.8 ^f
313	00:42:50.09 +41:22:05.7	0.6	0.6	70	35	NE	0.036±0.005	52/104	0.7 ^g
314	00:42:50.25 +41:18:12.9	0.2	0.3	73	31	NE=X	0.021±0.003	70/103	9.6 ^f
315	00:42:50.51 +41:07:50.9 ^a	1.5 ^a	1.5 ^a	42	33	[SSS]	0.031±0.006	37/74	0.0
316	00:42:50.76 +41:10:33.5	0.3	0.3	94	41	NE=GC	0.063±0.003 ^d	220/134	91.9 ^f
317	00:42:50.82 +41:17:07.4	0.4	0.3	68	40	NE=GC	0.031±0.003	86/107	0.0 ^f
318	00:42:50.82 +41:15:51.5	0.4	0.3	49	38	NE	0.014±0.002	52/86	0.4 ^g
319	00:42:51.206 +41:19:17.88	0.13	0.10	49	33	NE=T	0.022±0.003	658/81	1.3 ^f
320	00:42:51.34 +41:16:40.3	0.5	0.5	67	37	NE=X	0.026±0.004	107/103	0.0 ^g
321	00:42:51.46 +41:04:46.9	0.8	0.8	19	32	[*]	0.098±0.014	48/50	4.0
322	00:42:51.606 +41:17:01.42	0.13	0.10	52	21	NE=X,T	0.034±0.005	227/72	0.0 ^f
323	00:42:51.64 +41:15:11.8	0.3	0.3	70	34	NE	0.027±0.004	69/103	0.0 ^g
324	00:42:51.638 +41:13:02.76	0.13	0.10	106	55	H	0.182±0.005	374/160	0.6 ^g
325	00:42:51.73 +41:26:33.9	0.6	0.8	29	39	!AGN	0.177±0.012	55/67	7.4 ^f
326	00:42:51.816 +41:17:27.15	0.14	0.10	40	32	NE=T	0.014±0.003 ^d	141/71	11.8 ^f
327	00:42:52.03 +41:31:07.9	0.3	0.3	12	62	GC=BHC	44.0±0.2	587/73	0.0 ^f
328	00:42:52.308 +41:17:34.81	0.14	0.10	103	56	NE=X	0.076±0.003	195/158	0.3 ^g
329	00:42:52.34 +41:21:41.6	0.5	0.5	74	34	NE	0.032±0.004	55/107	0.0 ^g
330	00:42:52.433 +41:16:48.72	0.12	0.10	105	54	T	0.196±0.005	2941/158	9.6 ^f
331	00:42:52.467 +41:16:31.17	0.19	0.15	46	0	NE=T	0.007±0.002	171/45	0.3 ^f
332	00:42:52.52 +41:22:04.2	0.4	0.3	80	34	NE	0.061±0.005	182/113	35.3 ^f
333	00:42:52.525 +41:15:39.90	0.11	0.10	108	62	[SSS]=*	17.110±0.101	9252/169	128.6
334	00:42:52.53 +41:18:34.9	0.2	0.2	85	36	NE=X	0.04±0.00	94/120	0.0 ^g
335	00:42:52.534 +41:18:54.46	0.11	0.10	109	62	[XB]=BHC	10.15±0.07 ^c	441/108	0.0 ^f
336	00:42:52.63 +41:13:28.4	0.2	0.2	86	44	NE=X	0.035±0.003	86/129	0.0 ^g
337	00:42:52.63 +41:08:00.1	0.7	0.7	53	38	NE	0.037±0.005	63/90	0.0 ^g
338	00:42:53.07 +41:07:07.1	0.8	0.8	34	34	NE	0.050±0.010	47/67	1.8 ^g
339	00:42:53.173 +41:14:22.70	0.11	0.10	56	34	NE=X,T,U	0.015±0.002	37255/89	3.5 ^f
340	00:42:53.67 +41:29:47.1 ^a	1.4 ^a	1.4 ^a	13	45	H=[*],H	0.124±0.010	49/57	0.0 ^g

Table 1
continued.

Src	Pos	σ_{RA}''	σ_{Dec}''	O_A	O_H	Properties	$L_{con}/10^{37}$	χ^2/dof	SF Rank
341	00:42:53.68 +41:25:50.9	0.5	0.5	46	62	!SNR	0.337±0.009	442/107	3.3 ^f
342	00:42:53.7 +41:10:59 ^a	7 ^a	7 ^a	61	31	[SSS]	0.035±0.005	56/91	0.0
343	00:42:54.35 +41:13:33.9	0.4	0.4	54	33	NE	0.017±0.003	63/86	0.0 ^g
344	00:42:54.54 +41:04:00.5	0.6	0.7	11	38	NE=X	0.067±0.015	36/48	3.9 ^f
345	00:42:54.935 +41:16:03.19	0.11	0.10	109	62	H=BHC	3.12±0.03 ^c	5782/108	>320 ^f
346	00:42:55.18 +41:20:45.1 ^a	1.4 ^a	1.4 ^a	33	50	[SSS]	0.020±0.003 ^{d e}	173/82	126.3
347	00:42:55.197 +41:18:36.12	0.12	0.10	109	62	NE	0.417±0.007	605/170	133.1 ^f
348	00:42:55.41 +40:59:45.3	0.5	0.6	8	21	[SNR]	0.044±0.012	22/28	5.5 ^f
349	00:42:55.44 +41:25:57.2	0.2	0.2	46	62	NE	2.88±0.04	1666/107	149.1 ^f
350	00:42:55.629 +41:18:35.15	0.12	0.10	108	58	NE=GC	0.265±0.005	1051/165	>320 ^f
351	00:42:56.037 +41:12:18.43	0.13	0.10	34	28	NE=XB,T	0.010±0.002	564/61	0.0 ^f
352	00:42:56.84 +41:04:32.7	0.6	0.6	17	35	H	0.115±0.017 ^d	38/51	0.5 ^g
353	00:42:56.944 +41:18:43.95	0.12	0.10	66	47	T	0.060±0.004	1984/112	178.0 ^f
354	00:42:56.96 +41:04:21.2 ^a	1.9 ^a	1.9 ^a	13	36	H	0.068±0.014 ^d	41/48	3.6 ^f
355	00:42:57.00 +41:20:05.1	0.8	0.7	33	32	NE=T	0.015±0.002	399/64	26.0 ^f
356	00:42:57.18 +41:19:59.6	0.4	0.3	48	37	NE	0.011±0.002	60/84	6.5 ^f
357	00:42:57.39 +41:12:08.5	0.4	0.4	63	39	NE	0.022±0.004	74/101	6.4 ^f
358	00:42:57.900 +41:11:04.65	0.11	0.10	106	62	H=BHC	4.91±0.03	651/167	0.0 ^f
359	00:42:58.07 +41:13:19.3	0.3	0.3	57	31	NE	0.019±0.002	42/87	1.3 ^g
360	00:42:58.11 +41:13:37.2	0.2	0.2	81	39	NE	0.027±0.002	112/119	0.0 ^g
361	00:42:58.13 +41:16:52.2	0.6	0.7	60	33	NE=GC	0.024±0.004	60/92	0.0 ^f
362	00:42:58.317 +41:15:29.16	0.11	0.10	108	62	H	0.772±0.010	1402/169	83.9 ^f
363	00:42:58.63 +40:59:01.4	0.6	0.6	12	22	[*]	0.15±0.04 ^c	17/11	113.0
364	00:42:58.63 +41:11:59.1	0.5	0.4	80	33	H	0.040±0.004	74/112	0.0 ^g
365	00:42:58.647 +41:15:27.06	0.12	0.10	29	32	NE=T	0.006±0.002	503/60	0.0 ^f
366	00:42:58.97 +41:09:12.4	0.7	0.8	73	33	NE	0.069±0.007 ^d	69/105	0.0 ^g
367	00:42:59.03 +41:26:12.9	0.8	1.0	18	37	NE=X	0.037±0.010 ^d	49/54	2.4 ^g
368	00:42:59.27 +41:34:24.9 ^a	1.5 ^a	1.5 ^a	3	10	H	0.07±0.03	9/12	0.4 ^g
369	00:42:59.328 +41:16:42.94	0.19	0.10	39	46	[SSS]	0.022±0.003 ^e	223/84	0.8
370	00:42:59.36 +41:29:47.3	1.0	0.8	14	34	NE	0.090±0.009	65/47	4.3 ^f
371	00:42:59.52 +41:12:42.1	0.2	0.2	103	52	H	0.124±0.004 ^d	143/154	1.3 ^g
372	00:42:59.675 +41:19:19.35	0.11	0.10	107	62	GC=BHC	5.12±0.03	801/168	11.7 ^f
373	00:42:59.872 +41:16:05.72	0.11	0.10	108	62	GC=BHC	5.09±0.04 ^c	406/107	0.0 ^f
374	00:43:00.18 +41:08:43.1	0.5	0.4	74	44	[*]=*	0.053±0.005 ^d	69/117	0.5
375	00:43:00.80 +41:13:49.2	0.5	0.3	59	39	NE	0.022±0.002	72/97	0.7 ^g
376	00:43:01.110 +41:13:51.50	0.14	0.10	94	57	H	0.051±0.003	623/150	5.0 ^f
377	00:43:01.14 +41:13:17.3	0.2	0.2	64	45	NE	0.027±0.003	409/108	0.0 ^g
378	00:43:01.35 +41:30:17.0	0.6	0.6	14	62	GC	1.28±0.06 ^c	624/13	47.3 ^f
379	00:43:01.62 +41:10:52.5	0.3	0.4	87	44	[*]=*	0.044±0.003	85/130	0.0
380	00:43:01.69 +41:18:34.5	0.4	0.4	65	41	NE	0.027±0.003	59/105	1.2 ^g
381	00:43:01.72 +41:18:14.2	0.3	0.4	21	29	NE=X	0.011±0.003	47/49	11.1 ^f
382	00:43:01.78 +41:17:26.3	0.2	0.3	79	50	NE=[*]	0.016±0.003	47/128	0.0
383	00:43:02.27 +41:25:37.2	0.8	0.7	31	37	NE	0.044±0.007	44/67	0.8 ^g
384	00:43:02.44 +41:12:02.7	0.3	0.2	95	44	H	0.052±0.004	96/138	1.0 ^g
385	00:43:02.92 +41:06:45.1			16	35	NE	0.042±0.011	47/50	0.0 ^g
386	00:43:02.937 +41:15:22.53	0.11	0.10	109	62	GC=BHC	3.17±0.02	5245/170	>320 ^f
387	00:43:03.03 +41:20:42.2	0.2	0.2	102	52	H	0.195±0.006 ^d	279/153	42.4 ^f
388	00:43:03.13 +41:10:15.3	0.2	0.2	105	62	[GC]	0.836±0.015	1003/166	>320 ^f
389	00:43:03.220 +41:15:27.69	0.11	0.10	109	62	XB,BHC	1.462±0.015	14549/170	>320 ^f
390	00:43:03.327 +41:21:21.89	0.13	0.10	101	62	GC	3.19±0.05 ^c	1399/100	55.6 ^f
391	00:43:03.876 +41:18:04.91	0.11	0.10	108	62	GC=BHC	3.96±0.02	2885/169	13.7 ^f
392	00:43:04.15 +41:14:40.5	0.5	0.5	59	29	NE	0.026±0.005	51/87	3.3 ^f
393	00:43:04.244 +41:16:01.23	0.12	0.10	109	59	[GC]	0.401±0.007	1085/167	>320 ^f
394	00:43:04.80 +41:11:13.7	0.5	0.6	77	35	NE	0.040±0.004	77/111	1.0 ^g
395	00:43:05.17 +41:11:32.2	0.5	0.6	34	39	NE	0.015±0.005	12/72	1.8 ^g
396	00:43:05.667 +41:17:02.43	0.11	0.10	66	34	T=BHC	0.043±0.005	20445/99	2.0 ^f
397	00:43:06.38 +41:13:14.3	0.5	0.5	36	30	NE	0.016±0.003	38/65	0.6 ^g
398	00:43:06.64 +41:19:14.8	0.4	0.4	94	48	NC	0.138±0.007 ^d	121/141	0.0 ^g
399	00:43:06.75 +41:22:44.5	0.5	0.4	86	41	H=[*],H	0.076±0.006	88/126	0.0 ^g
400	00:43:07.01 +41:18:09.9	0.4	0.4	54	32	T	0.043±0.005	225/85	21.0 ^f
401	00:43:07.54 +41:20:19.6	0.2	0.2	100	60	[GC]=GC	0.386±0.008	813/159	320.0 ^f
402	00:43:07.60 +41:24:16.6 ^a	1.5 ^a	1.5 ^a	52	34	H=[*],[*]	0.045±0.006	59/85	1.2
403	00:43:08.32 +41:30:26.4 ^a	1.9 ^a	1.9 ^a	12	40	H	0.115±0.013 ^d	104/51	>320 ^f
404	00:43:08.35 +41:29:09 ^a	2 ^a	2 ^a	15	37	H=[*],H	0.076±0.011	92/51	2.4 ^g
405	00:43:08.49 +41:18:21.6 ^a	0.8 ^a	0.8 ^a	29	34	[SSS]	0.024±0.005	24/62	0.0
406	00:43:08.638 +41:12:48.30	0.13	0.10	105	61	X=XB	0.925±0.0150	655/165	2.7 ^f
407	00:43:08.85 +41:03:05.4 ^a	1.8 ^a	1.8 ^a	13	34	[SNR]	0.053±0.014	49/46	2.2
408	00:43:09.02 +41:07:30.8	0.5	0.7	25	55	[*]	0.045±0.005	128/79	21.1
409	00:43:09.57 +41:21:19.4	0.6	0.6	60	38	NE	0.034±0.005	61/97	0.0 ^g
410	00:43:09.61 +40:59:21.9	0.8	0.7	10	19	H	0.27±0.05 ^c	13/9	0.0 ^g

Table 1
continued.

Src	Pos	σ_{RA}''	σ_{Dec}''	O_A	O_H	Properties	$L_{con} / 10^{37}$	χ^2/dof	SF Rank
411	00:43:09.866 +41:19:00.76	0.14	0.10	91	55	T=[GC],BHC	0.120±0.006	2667/145	>320 ^f
412	00:43:09.97 +41:23:32.8	0.3	0.4	46	39	XB,T	0.042±0.005	282/84	23.5 ^f
413	00:43:10.07 +41:27:19.0	0.9	0.7	18	33	H	0.083±0.012	32/50	4.4 ^f
414	00:43:10.11 +41:17:20.3	0.5	0.7	60	29	[GC]	0.024±0.005	66/88	1.6 ^f
415	00:43:10.622 +41:14:51.30	0.11	0.10	103	62	H=GC,BHC	12.936±0.106 ^c	511/102	25.8 ^f
416	00:43:10.78 +41:30:43.0 ^a	1.1 ^a	1.1 ^a	10	36	H	0.064±0.015	38/45	0.0 ^g
417	00:43:11.31 +41:17:14.0	0.6	0.6	66	35	NE	0.030±0.005	70/100	0.0 ^g
418	00:43:11.37 +41:18:09.4	0.2	0.2	96	44	H	0.135±0.006 ^d	269/139	117.0 ^f
419	00:43:11.76 +41:06:04.9	0.9	0.7	11	41	NE	0.088±0.013	33/51	0.0 ^g
420	00:43:12.41 +41:20:32.3	0.4	0.7	63	39	NE=*	0.035±0.004	60/101	0.6
421	00:43:12.45 +40:58:56.3	0.6	0.5	9	20	H	0.29±0.04 ^c	11/8	0.0 ^g
422	00:43:12.97 +41:02:03.6	0.6	0.7	9	49	NE	0.190±0.018 ^e	773/57	0.0 ^g
423	00:43:13.11 +41:00:36 ^a	30	3	9	30	H	0.16±0.03 ^c	9/8	0.7 ^g
424	00:43:13.23 +41:18:13.4	0.2	0.2	96	56	H	0.153±0.006 ^d	362/151	44.8 ^f
425	00:43:13.87 +41:17:12.4	0.4	0.4	81	37	NE	0.058±0.005 ^d	76/117	0.0 ^g
426	00:43:14.13 +41:13:02.3	0.3	0.6	86	38	NE=var*	0.042±0.004	72/123	1.7
427	00:43:14.36 +41:07:20.8	0.2	0.3	25	62	GC	11.0±0.2 ^c	911/24	26.2 ^f
428	00:43:14.37 +41:16:50.1	0.3	0.2	97	44	H	0.080±0.005	115/140	0.0 ^g
429	00:43:14.60 +41:25:12.7	1.0	0.8	26	43	GC	0.061±0.007	58/68	1.7 ^f
430	00:43:14.60 +41:19:30.6	0.5	0.4	81	41	NE	0.048±0.004	75/121	0.0 ^g
431	00:43:15.04 +41:13:25.8	0.6	0.6	77	37	NE	0.040±0.004	62/113	0.0 ^g
432	00:43:15.46 +41:11:25.3	0.4	0.2	97	54	GC	0.155±0.007 ^d	245/150	221.0 ^f
433	00:43:15.50 +41:24:40.1 ^a	0.7 ^a	0.7 ^a	20	23	XB	0.030±0.011 ^d	37/42	2.4 ^f
434	00:43:16.12 +41:18:41.4	0.2	0.2	87	52	[XB]	0.099±0.005 ^d	551/138	225.0 ^f
435	00:43:16.40 +41:16:30.3	0.5	0.5	59	36	NE=[*]	0.028±0.004	49/94	0.0
436	00:43:16.51 +41:03:48.0	0.6	0.7	15	51	H	0.35±0.02	103/65	20.0 ^f
437	00:43:17.05 +41:12:24.1	0.5	0.4	65	44	NE=[*]	0.037±0.004	57/108	5.7
438	00:43:17.59 +41:27:44.9	0.3	0.3	15	62	NE=GC,BHC,T	0.01434±0.00014	3195/76	9.8 ^f
439	00:43:17.94 +41:11:13.1	0.6	0.6	55	46	H	0.038±0.005	63/100	0.0 ^g
440	00:43:18.52 +41:11:41.5	0.5	0.5	75	34	NE=X	0.043±0.005	72/108	0.0 ^g
441	00:43:18.77 +41:21:13.1	0.6	0.5	66	49	H	0.056±0.006	82/114	1.2 ^g
442	00:43:18.90 +41:20:17.0	0.4	0.4	84	50	[SSS]	0.096±0.006	859/133	5.1
443	00:43:19.23 +41:09:58.6	0.7	0.7	44	34	NE	0.040±0.006	40/77	0.0 ^g
444	00:43:19.52 +41:20:09.6	0.6	0.4	63	28	NE	0.034±0.004	79/90	0.0 ^g
445	00:43:19.520 +41:17:56.8 ^a	0.6 ^a	0.6 ^a	48	31	[SSS],T	0.023±0.004	92/78	9.3 ^f
446	00:43:19.97 +41:12:49.5	0.6	0.6	69	29	NE	0.037±0.005	69/97	0.0 ^g
447	00:43:20.64 +41:26:19.2 ^a	1.8 ^a	1.8 ^a	21	27	NC	0.064±0.010 ^d	47/47	4.2 ^f
448	00:43:20.740 +41:15:31.25	0.16	0.10	57	33	NE=T	0.031±0.005	3198/89	15.4 ^f
449	00:43:20.93 +41:18:51.4	0.4	0.5	86	37	NE	0.055±0.005	85/122	0.0 ^g
450	00:43:21.09 +41:17:50.5	0.2	0.2	103	60	H	0.639±0.011	1797/162	>320 ^f
451	00:43:21.25 +41:30:42.0 ^a	1.5 ^a	1.5 ^a	8	22	H	0.062±0.014	17/29	2.6 ^f
452	00:43:21.48 +41:15:56.6	0.6	0.5	71	43	NE=X	0.043±0.005	71/113	27.4 ^f
453	00:43:22.17 +41:09:23.5	0.6	1.0	26	21	NE	0.018±0.004	30/46	0.0 ^g
454	00:43:22.32 +41:12:56.2	0.4	0.4	82	32	NE=X	0.054±0.005	52/113	0.0 ^g
455	00:43:22.75 +41:20:42.1	0.6	0.5	61	34	NE	0.046±0.005	59/94	3.1 ^f
456	00:43:23.15 +41:06:00.2	0.7	0.7	10	36	H	0.098±0.016	21/45	1.0 ^g
457	00:43:23.44 +41:22:07.9 ^a	1.9 ^a	1.9 ^a	39	28	NC=[*]	0.049±0.008	41/66	0.0
458	00:43:23.67 +41:31:44.4 ^a	0.9 ^a	0.9 ^a	9	27	H	0.12±0.02 ^c	17/8	2.3 ^g
459	00:43:23.79 +41:04:27.5	0.7	0.7	12	35	NE	0.063±0.016	25/46	0.0 ^g
460	00:43:24.02 +41:13:13.3	0.4	0.5	83	29	H	0.057±0.007	76/111	0.0 ^g
461	00:43:24.85 +41:17:26.8	0.3	0.3	100	50	H	0.241±0.009 ^d	153/149	0.6 ^g
462	00:43:26.31 +41:19:11.2	0.5	0.4	78	40	[AGN]	0.200±0.009	96/117	0.0 ^g
463	00:43:26.65 +41:07:56.5	0.8	0.8	23	35	H	0.112±0.011 ^d	51/57	0.1 ^g
464	00:43:26.92 +41:14:04.3	0.6	0.5	52	29	NE	0.058±0.009 ^d	42/80	0.0 ^g
465	00:43:27.50 +41:10:18.3	0.8	0.7	35	34	NE	0.058±0.009 ^d	97/68	4.3 ^f
466	00:43:27.54 +41:12:25.8	0.7	0.7	61	34	NE	0.060±0.007 ^d	74/94	1.2 ^g
467	00:43:27.65 +41:06:43.1	0.8	0.7	14	39	H	0.074±0.014	32/52	0.0 ^g
468	00:43:27.91 +41:18:30.7	0.4	0.4	78	62	SNR	0.475±0.014 ^c	153/77	43.4 ^f
469	00:43:27.95 +41:05:03.3	0.5	0.6	13	46	H	0.116±0.014	44/58	0.0 ^g
470	00:43:28.69 +41:21:42.2 ^a	1.1 ^a	1.1 ^a	19	31	[SSS]	0.055±0.015	22/49	0.0
471	00:43:29.10 +41:07:47.4	0.5	0.4	23	62	H	8.98±0.19 ^c	50/22	4.6 ^f
472	00:43:29.54 +41:09:04.7	0.9	0.8	14	26	H	0.146±0.016	57/39	0.0 ^g
473	00:43:29.66 +41:19:55.0	0.5	1.0	36	26	NE	0.057±0.011	37/61	0.0 ^g
474	00:43:30.15 +41:03:09.2 ^a	1.3 ^a	1.3 ^a	5	39	[SSS]	0.141±0.018 ^e	349/43	13.1
475	00:43:30.25 +41:05:21.60	0.7	0.5	7	29	NE	0.08±0.02	25/35	0.2 ^g
476	00:43:31.29 +41:08:33.70	0.11	0.10	13	37	NE	0.075±0.017 ^d	60/49	0.6 ^g
477	00:43:32.24 +41:06:46.00	0.7	1.0	9	37	H	0.035±0.011 ^d	49/45	6.1 ^f
478	00:43:32.37 +41:10:40.70	0.2	0.3	35	61	H	7.48±0.13 ^c	91/34	0.0 ^g
479	00:43:32.713 +41:07:30.79			8	39	NE	0.074±0.014	35/46	21.1 ^f
480	00:43:33.59 +41:21:38.90	0.7	0.8	33	40	H	0.094±0.012 ^d	109/72	3.5 ^f

Table 1
continued.

Src	Pos	σ_{RA}''	σ_{Dec}''	O_A	O_H	Properties	$L_{con} / 10^{37}$	χ^2/dof	SF Rank
481	00:43:33.72 +41:14:06.30	0.7	0.9	38	34	H	0.100±0.012	60/71	0.0 ^g
482	00:43:33.86 +41:08:21.40	1.3	1.0	11	27	NE	0.112±0.015 ^d	42/37	5.2 ^f
483	00:43:34.29 +41:02:07.80	0.6	0.6	8	8	H	0.12±0.04 ^d	11/15	5.0 ^f
484	00:43:34.33 +41:13:23.10	0.2	0.2	50	62	H=BHC	3.77±0.04	1450/111	35.7 ^f
485	00:43:36.52 +41:09:25.20	0.9	1.4	14	34	NE	0.089±0.015 ^d	39/47	2.7 ^f
486	00:43:36.77 +41:08:12.00	1.3	1.0	9	38	GC	0.016±0.004	52/46	5.4 ^f
487	00:43:37.32 +41:14:43.10	0.2	0.2	40	62	GC=BHC	6.19±0.09 ^c	100/39	0.0 ^f
488	00:43:39.27 +41:26:53.0 ^a	0.7 ^a	0.7 ^a	26	51	!SNR	0.190±0.014 ^d	96/76	9.9 ^f
489	00:43:40.01 +41:19:49.60	1.1	0.8	23	28	NE	0.076±0.018 ^d	41/50	0.5 ^g
490	00:43:40.30 +41:00:44.20	0.9	1.3	5	10	H	0.16±0.06 ^c	1/4	0.0 ^g
491	00:43:41.53 +41:14:01.20	0.6	0.7	32	31	NE	0.082±0.011 ^d	59/62	4.3 ^f
492	00:43:41.95 +41:10:14.4 ^a	1.1 ^a	1.1 ^a	12	25	[*]	0.042±0.012 ^d	23/36	5.4
493	00:43:42.65 +41:26:07.10	0.7	0.7	4	18	NE	0.22±0.05	17/21	0.5 ^g
494	00:43:42.94 +41:28:49.90	0.8	0.7	19	29	[GC]	0.58±0.03 ^d	2048/47	7.9 ^f
495	00:43:43.89 +41:12:31.80	0.7	0.7	29	49	SNR	0.279±0.015	96/77	4.7 ^f
496	00:43:43.97 +41:03:38.90	1.9	0.9	5	11	NE	0.11±0.05	20/15	19.4 ^f
497	00:43:44.59 +41:24:10.20	0.7	0.6	32	47	NE=[XB],BHC,T	0.56±0.02	2578/78	50.6 ^f
498	00:43:44.66 +41:28:43.3 ^a	1.0 ^a	1.0 ^a	19	14	[AGN]	0.11±0.02	44/32	0.9 ^g
499	00:43:45.54 +41:27:09.3 ^a	1.2 ^a	1.2 ^a	17	51	H=[*],H	0.037±0.007	896/67	6.0 ^f
500	00:43:45.93 +41:12:04.1 ^a	1.1 ^a	1.1 ^a	26	48	H	0.154±0.011 ^d	57/73	1.0 ^g
501	00:43:46.31 +41:09:53.90	0.7	0.7	20	42	H	0.127±0.017 ^d	63/61	5.3 ^f
502	00:43:47.30 +41:27:44.5 ^a	0.8 ^a	0.8 ^a	14	18	[GC]	0.09±0.02 ^d	23/31	0.3 ^f
503	00:43:47.32 +41:06:53.90	1.1	1.0	18	50	H	0.26±0.02 ^c	35/17	0.0 ^g
504	00:43:49.57 +41:11:00.4 ^a	2 ^a	2 ^a	14	36	NC	0.053±0.014 ^d	40/49	0.0 ^g
505	00:43:50.28 +41:24:11.0 ^a	1.6 ^a	1.6 ^a	31	44	*	0.081±0.009	65/74	1.0
506	00:43:50.71 +41:21:18.60	0.5	0.6	43	47	H	0.43±0.02 ^d	175/89	0.0 ^g
507	00:43:51.85 +41:24:59.2 ^a	1.6 ^a	1.6 ^a	19	27	H=[*],H	0.062±0.012 ^d	34/45	0.1 ^g
508	00:43:53.62 +41:16:56.80	0.3	0.4	40	62	!GC	4.87±0.05	1534/101	124.4 ^f
509	00:43:53.69 +41:12:04.4 ^a	0.9 ^a	0.9 ^a	28	49	SNR	0.113±0.011	66/76	1.1
510	00:43:54.13 +41:20:47.3 ^a	2 ^a	2 ^a	26	31	[SNR]	0.042±0.009 ^d	41/56	2.2
511	00:43:54.40 +41:06:13.9 ^a	0.7 ^a	0.7 ^a	16	26	H	0.20±0.02	316/41	8.5 ^f
512	00:43:56.36 +41:22:01.5	0.6	0.6	42	57	GC	0.86±0.03 ^d	398/98	41.2 ^f
513	00:43:56.55 +41:06:44.9 ^a	1.1 ^a	1.1 ^a	10	26	H	0.21±0.03	258/35	4.7 ^f
514	00:43:58.25 +41:13:28.7 ^a	1.1 ^a	1.1 ^a	27	39	SNR	0.086±0.010 ^d	57/65	7.5 ^f
515	00:44:00.02 +41:13:44.7 ^a	1.8 ^a	1.8 ^a	21	28	[SSS]	0.037±0.010 ^d	21/48	0.0
516	00:44:01.03 +41:28:08.4 ^a	1.3 ^a	1.3 ^a	13	8	H	0.10±0.03 ^d	31/20	0.0 ^g
517	00:44:02.67 +41:17:17.4 ^a	2 ^a	2 ^a	35	32	H	0.079±0.010 ^d	67/66	0.0 ^g
518	00:44:03.23 +41:08:02.0 ^a	0.8 ^a	0.8 ^a	15	25	H	0.150±0.015	756/39	75.0 ^f
519	00:44:04.79 +41:21:27.7 ^a	1.0 ^a	1.0 ^a	37	21	[AGN]	0.217±0.016 ^d	49/57	14.9 ^f
520	00:44:09.41 +41:09:39.1 ^a	1.7 ^a	1.7 ^a	17	17	H	0.108±0.018	17/33	0.0 ^g
521	00:44:09.80 +41:20:11.7 ^a	1.1 ^a	1.1 ^a	27	20	[*]=*	0.107±0.014	63/46	0.9
522	00:44:13.55 +41:19:54.3 ^a	1.1 ^a	1.1 ^a	29	12	SNR	0.077±0.016 ^d	48/40	3.6 ^f
523	00:44:14.51 +41:22:04.1 ^a	0.7 ^a	0.7 ^a	21	17	[SSS]	0.159±0.021 ^e	391/37	4.0
524	00:44:16.99 +41:11:17.2 ^a	0.8 ^a	0.8 ^a	20	18	H	0.128±0.019	252/37	9.7 ^f
525	00:44:20.33 +41:21:37.1 ^a	1.6 ^a	1.6 ^a	16	7	[SSS]	0.056±0.020	9/22	7.9
526	00:44:24.18 +41:10:52.9 ^a	1.6 ^a	1.6 ^a	10	8	H	0.072±0.022	11/17	4.0 ^f
527	00:44:26.83 +41:15:02.5 ^a	1.8 ^a	1.8 ^a	17	6	[*]	0.057±0.024	14/22	0.0
528	00:44:27.03 +41:14:38.6 ^a	1.2 ^a	1.2 ^a	11	7	H	0.075±0.028 ^d	15/17	0.0 ^g

Table 2
continued.

Src	Model	$N_{\text{H}}/10^{22}$	χ^2/dof	Param	χ^2/dof
265	PO	0.137 ± 0.015	10/16	2.08 ± 0.04	11/17
266	PO	0.09 ± 0.03	1.4/7	1.60 ± 0.09	5/7
267	PO	0.06 ± 0.06	—	1.78 ± 0.19	—
268	PO	0.1 ± 0.10	—	2.7 ± 0.6	—
269	PO	0.106 ± 0.017	8/11	1.78 ± 0.05	10/11
270	PO	0.3 ± 0.2	0.8/2	1.7 ± 0.4	0.4/2
271	PO	0.23 ± 0.10	—	2 ± 0.2	—
274	PO	0.18 ± 0.04	0.9/6	2.13 ± 0.13	6/6
276	PO	0.42 ± 0.15	1.6/5	2.6 ± 0.3	2/5
277	PO	0.12 ± 0.09	0.18/1	2.1 ± 0.3	0.4/1
280	PO	0.10 ± 0.10	—	1.2 ± 0.2	—
286	PO	0.102 ± 0.015	5/13	1.61 ± 0.04	13/13
287	piled up DBB	$0.07 \pm f$	—	0.323 ± 0.014	—
289	PO	0.153 ± 0.018	26/65	1.58 ± 0.03	56/65
293	PO	0.13 ± 0.05	0.5/2	1.64 ± 0.10	0.9/2
297	PO	0.065 ± 0.014	8/17	1.91 ± 0.04	10/17
299	PO	0.115 ± 0.009	37/82	1.50 ± 0.02	57/82
300	PO	0.49 ± 0.04	17/19	1.84 ± 0.05	12/19
301	PO	0.12 ± 0.06	0.4/3	1.8 ± 0.2	2/3
306	PO	0.14 ± 0.03	3/8	1.68 ± 0.07	5/9
307	PO	0.17 ± 0.03	9/7	1.86 ± 0.09	13/7
322	PO	0.25 ± 0.25	—	2.5 ± 0.6	—
326	PO	0.22 ± 0.16	2e-5/2	2.3 ± 0.4	2e-5/1
327	PO	0.283 ± 0.011	40/14	1.89 ± 0.02	35/14
330	PO	0.06 ± 0.02	1.0/7	2.10 ± 0.11	2/7
333	BB	0.140 ± 0.014	13/14	0.0588 ± 0.0011	11/13
335	PO	0.214 ± 0.011	32/93	1.74 ± 0.02	47/93
339	DBB	0.102 ± 0.057	1.2/3	1.065 ± 0.09	16/3
345	PO	0.147 ± 0.011	23/70	1.7 ± 0.05	47/70
347	PO	0.16 ± 0.12	0.17/1	2.4 ± 0.4	0.6/1
349	PO	0.46 ± 0.06	2/7	1.84 ± 0.10	5/7
350	PO	0.08 ± 0.07	0.5/1	1.6 ± 0.2	2/1
353	PO	0.2 ± 0.2	—	1.6 ± 0.3	—
358	PO	0.149 ± 0.015	6/16	1.78 ± 0.04	13/16
362	PO	0.12 ± 0.04	3/8	1.76 ± 0.11	9/8
365	PO	0.22 ± 0.08	0.6/3	2.37 ± 0.19	0.8/3
368	PO	0.167 ± 0.02	7/18	1.78 ± 0.05	8/18
373	PO	0.09 ± 0.02	7/20	1.33 ± 0.03	12/20
378	PO	0.11 ± 0.07	3/4	0.80 ± 0.09	3/4
386	PO	0.15 ± 0.02	11/20	1.84 ± 0.05	18/20
388	PO	0.19 ± 0.09	0.7/4	1.25 ± 0.15	0.3/4
389	PO	0.159 ± 0.01	13/28	2.01 ± 0.05	12/28
390	PO	0.16 ± 0.08	0.8/4	2.18 ± 0.18	0.5/4
391	PO	0.15 ± 0.02	9/22	1.69 ± 0.04	15/22
393	PO	0.14 ± 0.06	0.4/5	1.98 ± 0.15	3/5
396	PO	0.08 ± 0.48	1.2/1	1.46 ± 0.08	18/1
406	PO	0.08 ± 0.04	0.7/4	0.82 ± 0.09	0.5/4
411	PO	0.29 ± 0.10	1.4/4	1.9 ± 0.2	3/4
415	PO	0.118 ± 0.01	30/96	1.47 ± 0.02	56/96
424	PO	0.11 ± 0.11	—	1.9 ± 0.4	—
427	PO	0.09 ± 0.04	7/11	0.52 ± 0.03	5/11
438	PO	0.12 ± 0.07	0.11/2	1.58 ± 0.2	0.13/2
448	PO	0.07 ± 0.00	—	0.64 ± 0.03	6/1
478	PO	0.87 ± 0.13	6/8	0.86 ± 0.10	4/8
484	PO	0.14 ± 0.03	10/9	1.94 ± 0.06	6/9
487	PO	0.13 ± 0.03	7/17	1.49 ± 0.05	8/17
497	PO	0.21 ± 0.06	4/7	1.81 ± 0.11	7/7
506	PO	0.14 ± 0.09	2/3	1.63 ± 0.3	1.2/3
508	PO	0.25 ± 0.02	19/17	2.74 ± 0.08	10/17
512	PO	0.3 ± 0.2	0.6/4	1.9 ± 0.2	0.6/4